ADVANCED OPTICAL MATERIALS
www.advopticalmat.de

Emerging Biomedical Applications of Organic Light-Emitting Diodes

Caroline Murawski and Malte C. Gather**

Dedicated to Professor Karl Leo on the occasion of his 60th birthday

As solid-state light sources based on amorphous organic semiconductors, organic light-emitting diodes (OLEDs) are widely used in modern smartphone displays and TVs. Due to the dramatic improvements in stability, efficiency, and brightness achieved over the last three decades, OLEDs have also become attractive light sources for compact and "imperceptible" biomedical devices that use light to probe, image, manipulate, or treat biological matter. The inherent mechanical flexibility of OLEDs and their compatibility with a wide range of substrates and geometries are of particular benefit in this context. Here, recent progress in the development and use of OLEDs for biomedical applications is reviewed. The specific requirements that this poses are described and compared to the current state of the art, in particular in terms of the brightness, patterning, stability, and encapsulation of OLEDs. Examples from several main areas are then discussed in some detail: on-chip sensing and integration with microfluidics, wearable devices for optical monitoring, therapeutic devices, and the emerging use in neuroscience for targeted photostimulation via optogenetics. The review closes with a brief outlook on future avenues to scale the manufacturing of OLED-based devices for biomedical use.

1. Introduction

Biophotonics—the use of light to image, investigate, manipulate, treat, or cut living matter—is seeing ever-increasing popularity for basic research and medical use.[1–3] In many cases, bulky lasers and optics are involved, but there is a growing demand for more compact devices that are biocompatible (potentially even bioresorbable and thus transient) and that for example can be implanted in animal models or worn by patients. Such devices would allow continuous monitoring and treatment, would enable the delivery of light to places that have been "dark" up until now, and would overall lead to a more "imperceptible" form of biophotonics. Great strides have been made in this direction, e.g., with the development of microendoscopes, yet the integration of light sources into this new type of biophotonics remains challenging.[4] Semiconductor LEDs and laser diodes become ever more compact and robust, but their integration with other optical and electronic components requires delicate assembly routines that are difficult to scale.

Organic light-emitting diodes (OLEDs) are a relatively young solid-state lighting technology. First demonstrated in the late 1980s and early 1990s,[5,6] they replace the crystalline III/V semiconductors used in conventional LEDs and diode lasers by organic π-conjugated molecules or polymers. The molecular nature of the light-emitting material means that the entire arsenal of organic chemistry is available to enhance and tune the properties of OLEDs.[7–9] In addition, most materials used in OLEDs today have an amorphous morphology and can be processed by thermal evaporation in high vacuum or even be printed.[10] This opens possibilities to tailor and optimize device performance through stacking and combination of materials and numerous types of optical optimization. [11–16] It also allows monolithic integration of OLEDs on a vast variety of substrates, from the large glass panels used by the display industry, to silicon chips with integrated photodetectors and data processing, to mechanically flexible plastic films and even fibers.[17,18]

These and other special properties of OLEDs make them highly attractive as light sources for the compact and "imperceptible"

Dr. C. Murawski
Kurt-Schwabe-Institut für Mess- und Sensortechnik Meinsberg e.V.
Kurt-Schwabe-Str. 4, 04736 Waldheim, Germany
E-mail: caroline.murawski@ksi-meinsberg.de
Prof. M. C. Gather
Humboldt Centre for Nano- and Biophotonics
Department of Chemistry
University of Cologne
50939 Köln, Germany
E-mail: malte.gather@uni-koeln.de
Prof. M. C. Gather
Organic Semiconductor Centre
SUPA
School of Physics and Astronomy
University of St Andrews
St Andrews KY16 9SS, UK
The ORCID identification number(s) for the author(s) of this article can be found under https://doi.org/10.1002/adom.202100269.

DOI: 10.1002/adom.202100269

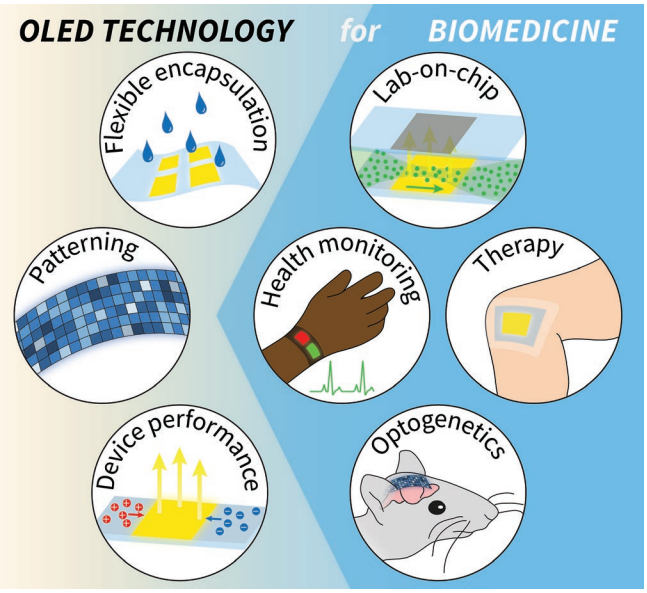

Figure 1. Schematic illustration of biomedical fields where OLED technology is poised to make a particularly significant impact, and key challenges associated with adopting OLED technology to these areas.

biophotonic devices discussed above. The opportunities for integration of OLEDs are vast, be it in thin plasters that double as optical pulse oximeters or local triggers of a light-activated chemotherapy, as drivers of all-optical neuronal interfaces, or to provide the probe light for an ultracompact spectrometer that can run quantitative immunoassays in low-resource settings (**Figure 1**). However, while research in this area is quickly gaining momentum, there are very substantial challenges. OLEDs have been developed for high-quality and potentially low-cost displays in TVs, computers, and mobile devices. It has taken the industry several decades to get OLED-based products to the market, in large part because the π-conjugated organic materials used are intrinsically susceptible to water, oxygen, light, and current.[19,20] For biomedical applications, there is frequently a need to make the devices more compact (leaving less space for an encapsulation that protects them from water and air), implant them in a warm and wet environment (e.g., on the human skin or in the brain of a mouse), and in some cases to operate them at brightness levels ten to a hundred times above even the brightest TV screen that exists today.

In this review, we discuss how scientists propose to address these challenges, which applications are now just beyond the horizon and where future challenges will be. We begin by describing the device requirements for biomedical applications, in particular in terms of flexibility, encapsulation, patterning, and peak brightness, before then discussing a set of biomedical applications of OLEDs. Specifically, we review the use of OLEDs as light source in on-chip sensors and spectrometers, in light-based wearable health monitors, as well as emerging uses in therapy and neuroscience. We deliberately focus exclusively on devices containing OLEDs and prioritize the OLED aspect in these devices. We have also mostly focused on biomedical applications and thus excluded a large and growing body of work on textile and wearable displays.

2. OLED Requirements for Biomedical Applications

The use of OLEDs in biomedical applications requires specific device properties that—compared to conventional display applications—pose additional challenges. Implementing OLEDs in wearable or even implantable devices requires high mechanical flexibility, which, at the same time, also needs to provide strong encapsulation in order to protect the devices from physiological environments. Additionally, some applications need miniaturization or patterning into high-density µm-scale pixels. The light intensity required may vary over several orders of magnitude: Wearable devices often work with light intensities well below the 100 µW mm^{-2} range; however, implantable devices used for stimulating and sensing cellular activity may require power densities up to 1 mW mm^{-2} or even higher. Sensing applications usually also benefit from reduced signal-to-noise at higher light intensities, however, also require low operating voltages to achieve low power consumption and allow integration with standard driver electronics; e.g., complementary metal oxide semiconductor (CMOS) integrated circuits (ICs), which are the standard in silicon electronics, frequently operate at 5 V. Thus, steep current–voltage curves and high external quantum efficiencies are of particular benefit for biomedical applications. The spectral requirements strongly depend on the application, with emission colors spanning the whole visible range up to the infrared. Several applications, especially in the field of optical sensing, require narrower emission spectra than what is offered by conventional OLED emitter materials—an aspect that we will discuss in more detail in Section 3.1 when reviewing lab-on-chip OLED applications.

2.1. Flexibility and Encapsulation

Mechanical flexibility is one of the key advantages of OLEDs over conventional light sources. However, achieving robust flexible OLEDs is extremely challenging and extensive research has looked into their development.[18,21,22] One of the bottlenecks in realizing high flexibility is the electrodes involved since the conventionally used indium tin oxide (ITO) is brittle and quickly breaks under the bending strain.[23] The probably most common alternative is 15–30 nm thin metal layers. While these suffer from reduced transparency compared to ITO, using even thinner metal layers leads to strongly increased sheet resistance due to island growth. In order to prevent island formation during metal deposition and thus improve transparency and conductivity, e.g., of very thin silver films, nanometer thin seed layers with high surface energy such as gold can be used to enable closed Ag layers at a thickness of only 4–7 nm.[24–27] Alternatives comprise the use of dielectric/metal/dielectric films,[28–30] where common dielectrics are high-refractive index materials such as MoO_3, WO_3, and ZnS. Other flexible transparent electrode materials include conductive polymers,[31,32] graphene,[33–35] carbon nanotubes,[36,37] metal nanowires,[38–41] and metal meshes[42,43] as reviewed in refs. [22,44–47].

OLEDs can be fabricated on extremely thin substrates down to 1 µm, and such devices can achieve bending radii of 100 µm or less.[40,48–52] Additionally, stretchable OLEDs have gained a lot of attention and are extremely promising for wearable devices,

which usually experience both bending and tensile strain.[48,52–58] Despite the great promise in achieving highly flexible light-emitting devices, the use of OLEDs in medicine typically requires device lifetimes ranging from few hours in case of plaster-type wearables up to years when used as implants. In addition, for many applications the devices have to withstand harsh environmental conditions, in particular high humidity and/or immersion into water. Since organic materials very quickly degrade in contact with moisture or oxygen, the devices need to be protected with robust thin-film encapsulation (TFE) layers. Typically a water vapor transmission rate (WVTR) well below 10^{-5} g m^{-2} day^{-1} is seen as a requirement for OLEDs.[59]

Atomic layer deposition (ALD) of amorphous metal oxides is considered one of the best strategies to deposit conformal, pin-hole free encapsulation layers.[60] In particular the use of nanolaminates—few nanometer thick alternating layers of two different oxide materials—showed promising WVTRs, i.e., on the order of 10^{-5} g m^{-2} day^{-1}.[61–65] However, inorganic encapsulation layers, especially the conventionally used Al_2O_3, quickly deteriorate in high humidity.[66,67] Instead, multilayer inorganic/polymer structures may be used to prevent direct contact of the inorganic layer with water and these have indeed shown superior protection.[67–70] The application of OLEDs as wearable sensors or for medical treatment requires the devices to keep working also when their owner takes a shower or goes for a swim. Functional implants furthermore require OLEDs that work in physiological environments for months and years. The use of additional organic protection layers also helps to adjust the position of the inorganic layers within the multilayer stack, i.e., allows to place them as close as possible to the neutral plane of the device. This may reduce the stress that is exerted onto these rather brittle layers upon bending.[50,71]

So far, only few studies have addressed the need for water-resistant, flexible OLEDs. Song et al. developed OLED fibers that can be interwoven to form a textile-like display (**Figure 2**a,b).[72] The design allowed consistent unidirectional stretchability up to 20% strain. Using a passivation layer consisting of 50 nm of thermally evaporated MoO_3 and around 100 µm of a polyurethane-based polymer, the authors also achieved some device stability in water, with a luminance decrease to 50% of the initial value after approximately 2 h. Jeong et al. demonstrated flexible, washable OLEDs and organic solar cells (Figure 2c,d).[61] Using an encapsulation barrier with 3 dyads of ALD-deposited Al_2O_3/ZnO nanolaminate and an SiO_2–polymer composite material, both deposited onto a PET film that was subsequently attached on top of the devices, the OLEDs and solar cells resisted up to 20 washing cycles in aqueous detergent for 10 min each without significant degradation. Similar resistance to repeated washing cycles was obtained with 10 µm thin OLEDs that were fabricated on and encapsulated with 4.8 µm thin barriers.[73] These films consisted of a PET film containing an acrylic for simple adhesion to surfaces and a 2 dyad encapsulation of ALD-deposited ZnO, Al_2O_3, and MgO (ZAM)[64] and a Si-based polymer.

Recently, we developed substrate-less, 12 µm thin, highly flexible OLEDs embedded in between hybrid TFE barrier layers consisting of two dyads of the polymer parylene-C and an Al_2O_3/ZrO_2-nanolaminate deposited by ALD (Figure 2e–h).[74] Parylene-C is a widely used and FDA-approved protective coating for biomedical devices and has also been used as a substrate for flexible OLEDs.[51,52,69,75] These substrate-less OLEDs resisted repeated bending and showed no significant degradation when immersed in DI water and cell nutrient solutions for more than 2 weeks. Additionally, the encapsulation withstood harsh postprocessing, including a bath in organic solvents, photolithography, and reactive gas plasmas.

2.2. Miniaturization and Patterning

Biomedical applications of OLEDs often require miniaturization or patterning of the devices to create high-density light-emitting arrays. Currently used techniques to integrate or pattern OLEDs for biomedical applications include the assembly of separate components deposited onto different substrates,[52,76] material evaporation through shadow masks,[77,78] photolithographic patterning of the bottom electrode,[79] and blade-coating.[80] Patterning of OLEDs to high-density micrometer scale pixels, however, remains a challenge and an active area of research for the organic community. In the following, we review some strategies that may be particularly applicable to miniaturizing and/or patterning OLEDs for biomedical applications.

Conventionally, the active pixel area in vapor-deposited devices is defined using fine metal masks (FMM). This is also the dominant method used for high-resolution commercial displays, e.g., for smartphones. However, the resolution typically remains below 1000 ppi due to mask sagging and material diffusion into the gaps. On a laboratory scale, patterning with shadow masks is further constrained due to difficulties with mask alignment and is hence often limited to structure sizes well above 100 µm. An extension of FMM is stencil nanolithography, which uses a polymeric membrane mask that is transferred directly onto the substrate and which can achieve feature sizes down to 500 nm.[81] Patterning of a dielectric insulating layer deposited either below or on top of the organic layers is a commonly used alternative to mask the active area.[82,83] However, integration of multiple miniaturized devices onto a common substrate and patterning these to micrometer-scale dimensions require other strategies.

Photolithography—the gold standard in conventional (inorganic) microelectronics—cannot be readily applied to organic materials due to the incompatibility of organic materials with most solvents and photoresists. One strategy to apply photolithographic patterning to conventional organic semiconductor materials is hydrofluoroethers.[84] These orthogonal solvents are chemically benign to organic materials[85,86] and compatible with the patterning of complete multilayer state-of-the-art OLEDs (**Figure 3**a,b).[87–89] As an alternative to using fluorinated resists, nonfluorinated photoresists in combination with reactive ion etching using oxygen plasma were reported for patterning of organic photodetectors.[90] In order to apply conventional photolithography on top of OLEDs, the organic layers may be protected by dielectric passivation layers.[74,91,92] Using this strategy, Choi et al. recently developed a thin-film-transistor driven OLED display that incorporated vertically stacked RGB sub-pixels (Figure 3c,d).[92] Each subpixel contained an Al_2O_3 TFE-layer and an additional SiN_x passivation layer deposited by plasma-enhanced chemical vapor deposition. This protection of

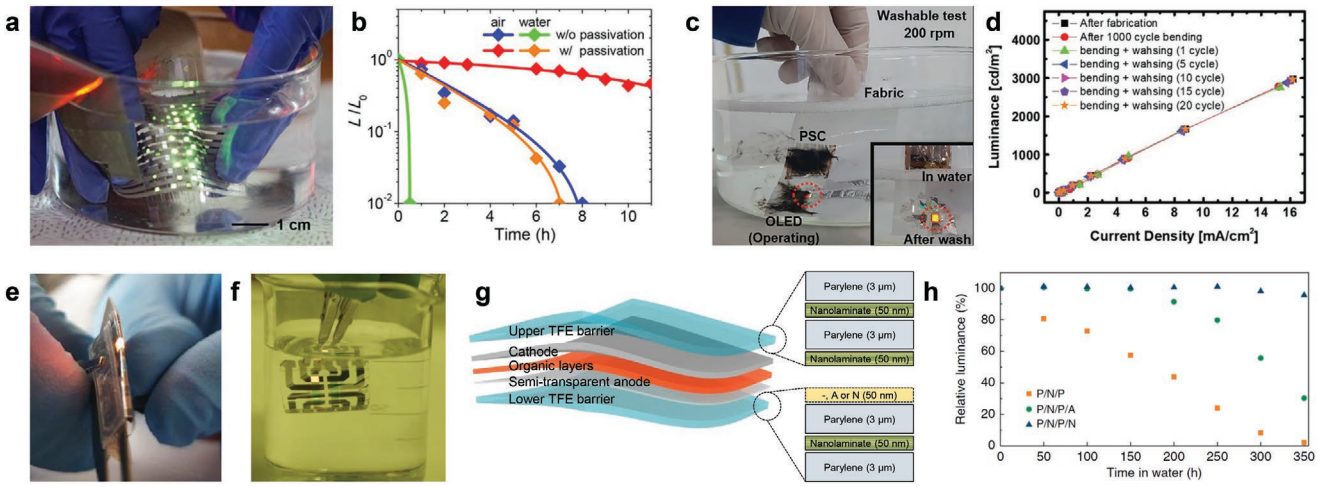

Figure 2. Flexible OLEDs for use in aqueous environments. a) Textile OLED display with interwoven fibers immersed in DI water. b) Degradation of the textile OLED display with and without passivation layer in water and air. a,b) Reproduced with permission.[72] Copyright 2020, American Chemical Society. c,d) Photograph of washable OLEDs and luminance over current density after repeated bending and washing steps. Reproduced with permission.[61] Copyright 2019, The Royal Society of Chemistry. e,f) Substrate-less, flexible, water-proof OLEDs bent around the backside of a razor blade and operated in DI water. g) Schematic of a substrate-less OLED with hybrid TFE consisting of parylene and Al_2O_3/ZrO_2-nanolaminate structure. h) Luminance degradation of substrate-less OLEDs with different compositions of lower TFE barrier layers (P: parylene-C, N: nanolaminate, A: Al_2O_3). e–h) Reproduced and adapted under the terms and conditions of the CC-BY 4.0 license.[74] Copyright 2020, The Authors, published by Springer Nature.

the organic materials facilitated subsequent patterning of the indium zinc oxide (IZO) electrode by photolithography and etching.

Conventional photolithography may also be used to directly pattern photosensitive polymer layers. For this, selective cross-linking of the polymer by UV-lithography may be enabled by attaching oxetane side groups.[93,94] This concept can also modulate layer thicknesses via grayscale lithography, which can be used for selective narrow-band light outcoupling from microcavity OLEDs.[95] Using a white emission layer, it is thus possible to achieve RGB patterning from a single OLED structure (Figure 3e). The same microcavity approach was applied in another study on vapor-deposited OLEDs, where the thickness of a p-doped hole transporting material was modulated using electron beam lithography.[96] As an alternative to making use of microcavity effects, Joo et al. recently introduced metasurfaces for selective outcoupling of narrow-band emission from white OLEDs.[97] For this, OLEDs were deposited onto reflective nanopillars and the emission spectrum was tuned by varying the pillar diameter and pitch (Figure 3f,g). This strategy enabled pixel densities exceeding 10 000 ppi and improved luminescence efficiency compared to color-filtered white OLEDs.

Printing techniques have a great prospect for scalability and patterning. However, most printing techniques deposit organic semiconductors from solution, which often leads to inferior device efficiency and lifetime compared to vapor deposited devices due to reduced thickness control and difficulties with multilayer deposition. Wet printing techniques with patterning ability include inkjet printing,[98–101] gravure printing,[100,102] and aerosol jet printing,[103] which achieve minimum pattern sizes of 5– 30 µm.[102,104] Instead, dry printing techniques such as organic vapor jet printing (OVJP)[105–107] and transfer printing[108–112] can be used to fabricate complex multilayer stacks using small molecule materials. The latter method allows the transfer of individual layers and of whole OLEDs using an elastomeric stamp and can achieve sub-micrometer scale feature sizes (Figure 3h).[108]

2.3. Device Performance

Improving the external quantum efficiency (EQE) of OLEDs is considered one of the most important challenges of OLED research. Since three quarters of the excited states in OLEDs are "dark" triplet states that require a spin flip to become luminescent, the development of new light-emitting compounds based on either phosphorescence or thermally activated delayed fluorescence (TADF) has caught significant attention.[113–116] High EQE is indeed an important factor for device optimization, however, it is less relevant for biomedical applications, which instead require high absolute light intensities, low power consumption, and low levels of device heating.

In contrast to display and lighting applications, the light intensity required for biomedical applications is independent of human vision and thus quantified in radiometric units. So far, however, OLED development mainly targeted vision-centric applications and thus most literature reports only provide photometric quantities such as device luminance. In order to convert photometric quantities into radiometric data, the spectrum needs to be multiplied with the photopic luminosity function, V_λ, which peaks at 555 nm and significantly decreases toward the blue and red spectral region.[117] **Figure 4**a shows representative conversions between optical power density and luminance as a function of the peak wavelength of the emission spectrum. This has been calculated by using the shape of a typical OLED emission spectrum (based on the emitter $Ir(ppy)_3$) with a full width at half maximum (FWHM) of 77 nm and shifting the spectrum along the wavelength axis. Since

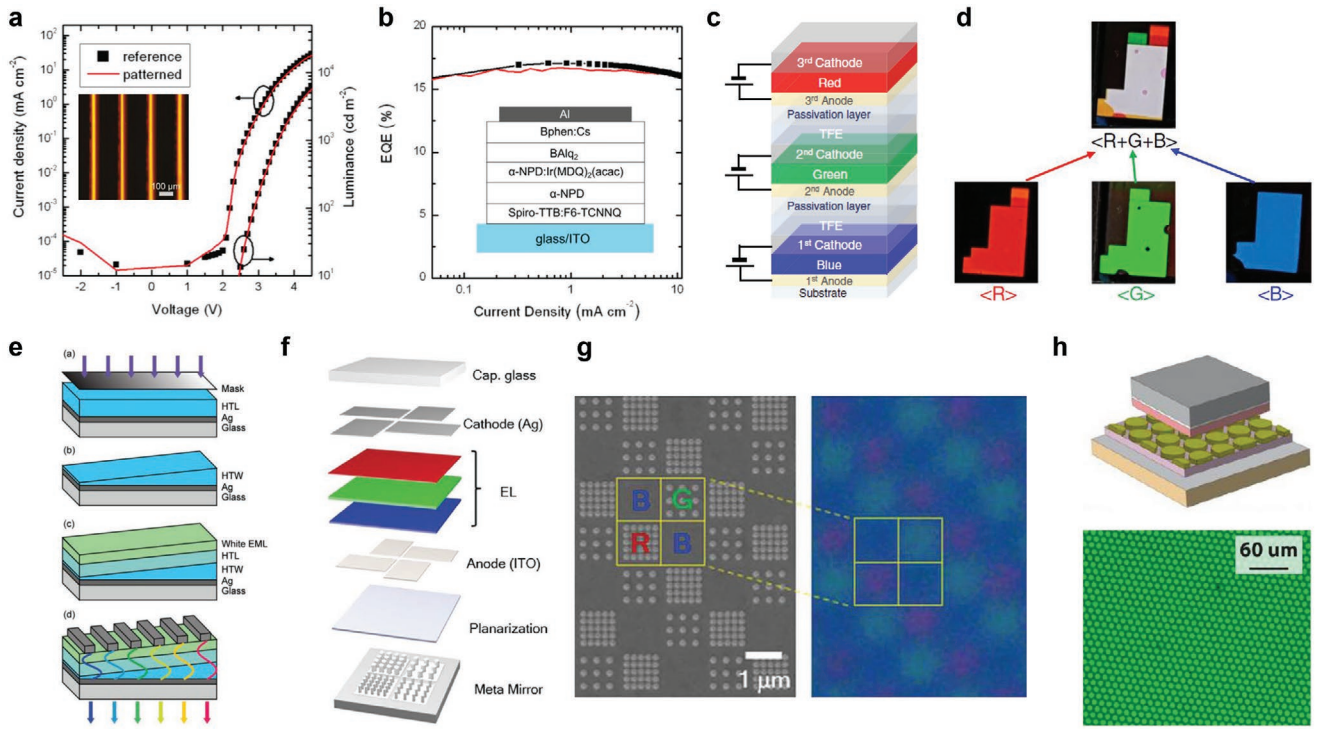

Figure 3. Strategies for OLED patterning with particular relevance to biomedical applications. a,b) Photolithographic patterning of state-of-the-art OLEDs using orthogonal resists and fluorinated solvents. Reproduced with permission.[87] Copyright 2014, John Wiley and Sons. c,d) Thin-film transistor-driven vertically stacked RGB-pixels patterned by protecting devices with dielectric TFE and further passivation layers. Reproduced under the terms and conditions of the CC-BY 4.0 license.[92] Copyright 2020, The Authors, published by Springer Nature. e) Selective light outcoupling from white-emitting material by modulation of an OLED microcavity using grayscale lithography. Reproduced with permission.[95] Copyright 2010, John Wiley and Sons. f,g) Metaphotonic color selection from white OLEDs enables pixels on micrometer scale. Reproduced with permission.[97] Copyright 2020, AAAS. h) Patterning of the emission layer by transfer printing. Reproduced with permission.[108] Copyright 2016, American Chemical Society.

OLEDs may also have significantly narrower spectra, we additionally calculated the luminance for spectra with a FWHM of 38 nm. These simple calculations indicate that a power density of 1 mW mm^{-2} is achieved at ≈70 000 cd m^{-2} for blue OLEDs (peak: 457 nm), at ≈160 000 cd m^{-2} for green OLEDs (peak: 527 nm), and at ≈46 000 cd m^{-2} for red OLEDs (peak: 617 nm) when considering the broad spectrum. For the narrower emission spectrum, the luminance required to reach a certain power density is significantly lower for blue OLEDs but slightly higher for green- and red-emitting devices. We note that these values only give a rough estimate since the actual conversion strongly depends on the specific spectral shape and the angular emission profile of the device. Hence, conversions should always be made using measurements of the angle-resolved electroluminescence spectra.

While very high EQE may be reached with phosphorescent and TADF materials even at high luminance of 10 000 cd m^{-2},[113,118–122] the harvesting of triplet excitons brings about several additional challenges for high brightness applications. First, triplet excited states possess long lifetimes (microseconds or longer). As a result, high drive currents lead to very high triplet densities, which are prone to bimolecular annihilation processes.[123–126] Thus, phosphorescent and TADF materials typically suffer from much stronger efficiency roll-off compared to fluorescent materials, i.e., their EQE strongly drops at increasing drive currents and may even fall below the EQE of a respective fluorescent material.[127] Second, triplet-triplet annihilation leads to the formation of higher lying triplet excitons, which are particularly reactive.[128–130] As a consequence, especially blue triplet harvesting emitters suffer from pronounced intrinsic degradation and most often do not reach high luminance. Third, the use of phosphorescent and TADF emitters most often requires host materials with high triplet energy. Consequently, those materials possess larger bandgaps and thus devices based on them typically require higher drive voltages than those using fluorescent emitters. (Note that there is increasing research on using nondoped phosphorescent[131] and TADF emitters,[132,133] which may reduce drive voltages compared to host–guest systems.[133]) Low drive voltages are important for biomedical applications, not only for reducing power consumption and for integration with electronic drivers, but also for reducing resistive heating of the environment. Especially applications involving direct contact of the light source with live cells and in particular brain tissue need to retain the environment at physiological temperatures, which means that only a temperature increase up to around 1 °C is tolerated.

In the following, we review selected reports that achieved particularly high optical power density, i.e., exceeding 1 mW mm^{-2}, at relatively low voltages. Note that due to the reasons discussed above and because most OLED research is dedicated to display and lighting applications, which require not more than

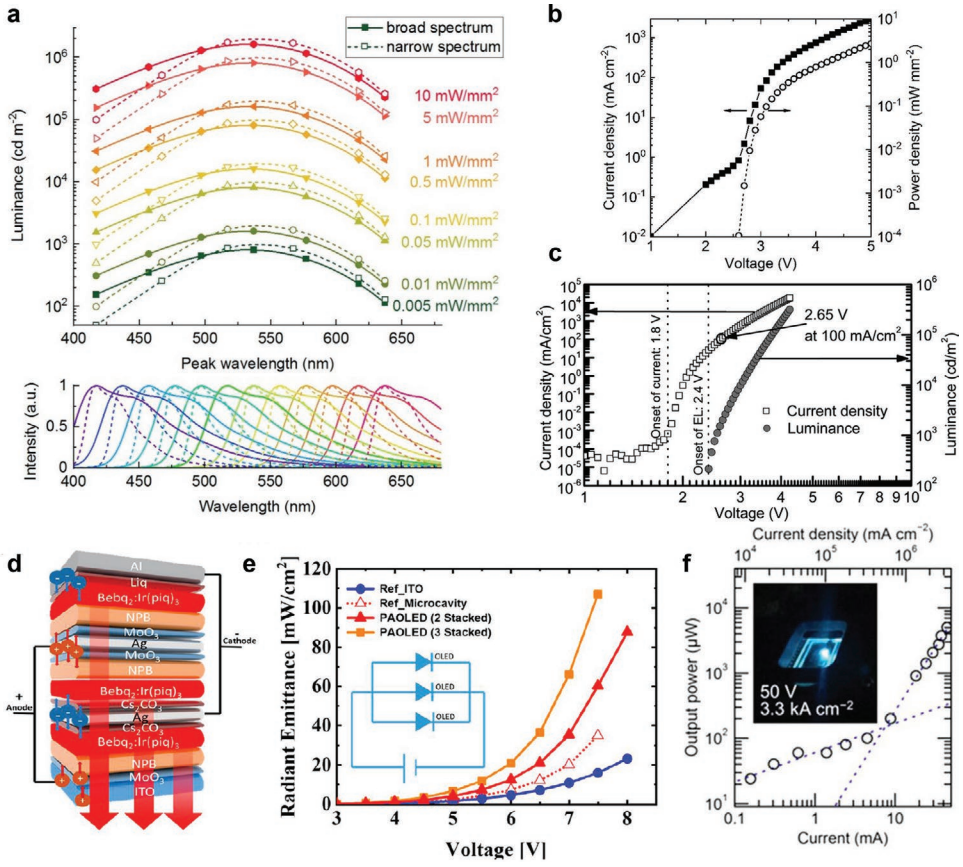

Figure 4. Development of OLEDs with high power density. a) Conversion between optical power density and luminance (top). Conversion depends on the spectral shape (bottom; broad spectra have a FWHM of 77 nm (solid lines); narrow spectra have a FWHM of 38 nm (dashed lines)) and is plotted as a function of the peak wavelength. Conversion assumes OLEDs with Lambertian emission characteristics. b) Fluorescent blue pin-OLEDs achieving an optical power density of 2.4 mW mm^{-2} at 5 V. Adapted with permission.[138] Copyright 2020, Wiley. c) Fluorescent green-emitting pin-OLEDs reaching 300 000 cd m^{-2} at 4.3 V. Reproduced with permission.[140] Copyright 2008, American Institute of Physics. d,e) Stacked red-emitting OLEDs with parallel connection of subunits reaching high power output and improved device lifetime. Reproduced with permission.[144] Copyright 2020, American Chemical Society. f) Output power versus current density of an OLED showing many of the characteristics of an electrically driven laser. Reproduced under the terms and conditions of the CC-BY 4.0 license.[148] Copyright 2019, The Authors, published by Japan Society of Applied Physics.

500–10 000 cd m^{-2}, reports on OLED performance at very high luminance (>50 000 cd m^{-2}) are scarce.

Very steep current density–voltage curves may be achieved using the so-called pin-concept, i.e., electrically doped charge transport layers.[13,134–137] This strategy enables efficient charge carrier injection, restricts voltage losses to the thin intrinsic layers, and makes it possible to adjust the thickness of the doped layers to optimizing outcoupling efficiency and controlling the emission spectrum. While pin-OLEDs often achieve orders of magnitude higher currents compared to nondoped devices at a given voltage, further reduction of internal and external voltage losses may be possible by minimizing the thickness of the intrinsic layers and reducing in-plane resistive losses in the ITO electrode, respectively.[138] Based on this strategy and using the fluorescent blue emitter 2,5,8,11-tetra-*tert*-butylperylene (TBPe), we recently built OLEDs that achieved current densities of 3000 mA cm^{-2} at 5 V. Although the EQE of the devices was only 4.4 % at maximum, the extremely high current density led to a luminance of 132 000 cd m^{-2} and a light power output of 2.4 mW mm^{-2} at only 5 V (Figure 4b).[138]

High luminance from blue, fluorescent OLEDs was also shown using phenanthroimidazole-pyrene derivatives in a nondoped emission layer. The OLEDs reached up to 54 300 cd m^{-2} at 448 nm peak wavelength, albeit at significantly higher voltages (>10 V).[139] Another study used the blue fluorescent emitter p-bis(p-*N,N*-diphenyl-aminostyryl) benzene (DSA-Ph) to fabricate OLEDs with a peak emission at 464 nm and low FWHM of 22 nm that reached 40 500 cd m^{-2} at 6.5 V.[73] Furthermore, fluorescent green OLEDs were developed that achieved around 300 000 cd m^{-2} at only 4.3 V—clearly exceeding 1 mW mm^{-2}—based on the emitter alpha-sexithiophene (α-6T) and doped charge transport layers (Figure 4c).[140] Although the external quantum efficiency of those devices was only 0.69 %, no efficiency decrease was observed even at the highest luminance.

Stacked OLEDs that are connected in series using an intermediate charge generation layer can enhance power output and lifetime, however, require higher drive voltage.[141–143] Parallel connection of stacked OLEDs instead makes it possible to achieve high power output and lifetime while keeping operating voltages low. This concept was recently employed

in flexible, red-emitting phosphorescent OLEDs based on the emitter $Ir(piq)_3$ (Figure 4d,e).[144] By stacking three OLEDs, optical power densities up to 1 mW mm^{-2} and improved device lifetime compared to individual OLEDs was achieved at an operation voltage of 7.5 V.

In order to increase drive currents further, designs should consider methods to reduce thermal load by using substrates with high thermal conductivity and by reducing the active area.[83,138,145–147] A reduction of the active area down to nanoscopic sizes (50–200 nm) furthermore reduces exciton annihilation, which may strongly reduce efficiency roll-off and thus improve light output at high drive currents.[83,147] However, the required device area is often determined by the application and the attachment of heat sinks is hardly possible for flexible, wearable, or transparent devices. Alternatively, pulsed-mode driving schemes strongly improve heat dissipation, which makes it possible to operate OLEDs at current densities up to few kA cm^{-2},[83,146,148,149] and this is already used in some biomedical applications.[49,150,151] Sandanayaka et al. recently reported on an OLED that shows the typical characteristics of an electrically driven laser.[148] This OLED was based on the blue fluorescent emitter BSBCz and was deposited on a distributed feedback grating. Using a pulsed-mode driving scheme with 1 kHz pulses of 400 ns length, the authors achieved current densities of 3.3 kA cm^{-2} at 50 V. This led to lasing with an optical power output of 0.5 mW, which corresponds to a record power density of 185 mW mm^{-2} (device area: 30 μm × 90 μm; Figure 4f). While this demonstrates the potential of OLEDs for extremely high-brightness applications, the device active area and the ultrashort voltage pulses used will not be suitable for many biomedical applications.

Further improvement of device power output may be achieved by increasing the light outcoupling efficiency, e.g., through incorporation of internal or external scattering structures, the attachment of optical elements, using materials with low refractive index, and emitters with horizontally oriented transition dipole moments, as reviewed in refs. [152–155]. However, bulky optical elements are incompatible with flexible substrates and the use of scattering structures will reduce the resolution of micropatterned devices, so outcoupling structures need to be selected according to the targeted biomedical application.

3. Emerging Biomedical Applications

3.1. OLEDs for Lab-On-Chip Applications

Because lab-on-chip use of organic electronics and OLEDs has been summarized in a number of older reviews,[156–159] we limit the following discussion to the main concepts and to recent developments. We also restrict our discussion to work using OLEDs in some form and do not cover fluorescence-based sensing modalities that use organic materials but note that in some cases these materials are similar to the emissive materials in OLEDs.

The advances in microfluidics over the last few decades have led to new opportunities for compact and low-cost lab-on-chip sensors, with applications ranging from outpatient and at-home testing of patient samples to food and agriculture and to the chemical industry. In many cases, these sensors can be read out directly through a visual signal detectable by eye, most often a color or intensity change. However, this is often limited to a yes/no answer and accurate quantification of, e.g., the concentration of an analyte remains challenging. Here, integration of optics and optoelectronics into lab-on-chip devices can add additional functionality. While the integration of passive optical components—in particular waveguides and gratings—with microfluidics is well established, the integration of active devices, i.e., light sources and light detectors, is more challenging as these are less compatible with the plastic, glass, or sometimes paper-based material platforms of lab-on-chip systems.

In this context, organic electronics offer the benefit of allowing direct monolithic integration on a wide range of substrates, which is principally due to the amorphous structure of organic semiconductors. (By contrast, most conventional electronic components require a pick-and-place approach for device assembly due to lattice matching constraints.) In addition, organic electronics offer potentially much lower cost of manufacture and reduced environmental burden, both of which are particularly important for single-use sensors that are deployed in situations where adequate waste disposal may not be available.

So far, the majority of on-chip systems using OLEDs have used a stacked configuration, with a microfluidic chip in the center, sandwiched by OLED light sources on one side and—at least in most cases— by organic photodiodes (OPD) or silicon-based photodetectors on the opposite side (**Figure 5**a). There are some examples, however, where OLEDs have been integrated on top or inside optical waveguides to realize more complex optical functionality.[160–162]

Two main measurement principles have been employed for on-chip sensing with OLEDs: sample transmission/absorption[95,163,164] and detection of photoluminescence from a compound in the sample.[78,164–176] Both modalities can be set up to record signals at different wavelengths and can multiplex several analytes in parallel, e.g., through the use of multiple microfluidic channels on a chip.

Measurement of sample transmission/absorption is ostensibly somewhat simpler than detection of photoluminescence because 1) lower light intensity is required and 2) there is no need to filter out direct excitation light from the OLED in the detected signal (see below). However, to yield meaningful results, transmission measurements frequently require many orders of magnitude in dynamic range. (e.g., commercial UV/Vis spectrometers routinely detect optical densities between 0.01 and 4.) Therefore, suppression of stray light and low noise operation of both light source and detector are important to obtain reliable data.

Fluorescence detection can be more specific than absorption as generally only the species of interest will emit substantial fluorescence under photoexcitation in a specific spectral band. However, as the interaction length of light with the analyte tends to be short in microfluidic devices (sub-mm) and analyte concentrations are often low (sub-10^{-4} M), fluorescence is usually many orders of magnitude weaker than the excitation light. Detection therefore requires an efficient scheme to reject excitation light from the detector. One strategy to achieve this rejection is the use of crossed polarizers, i.e., to excite the sample with highly polarized light and pass the resulting largely

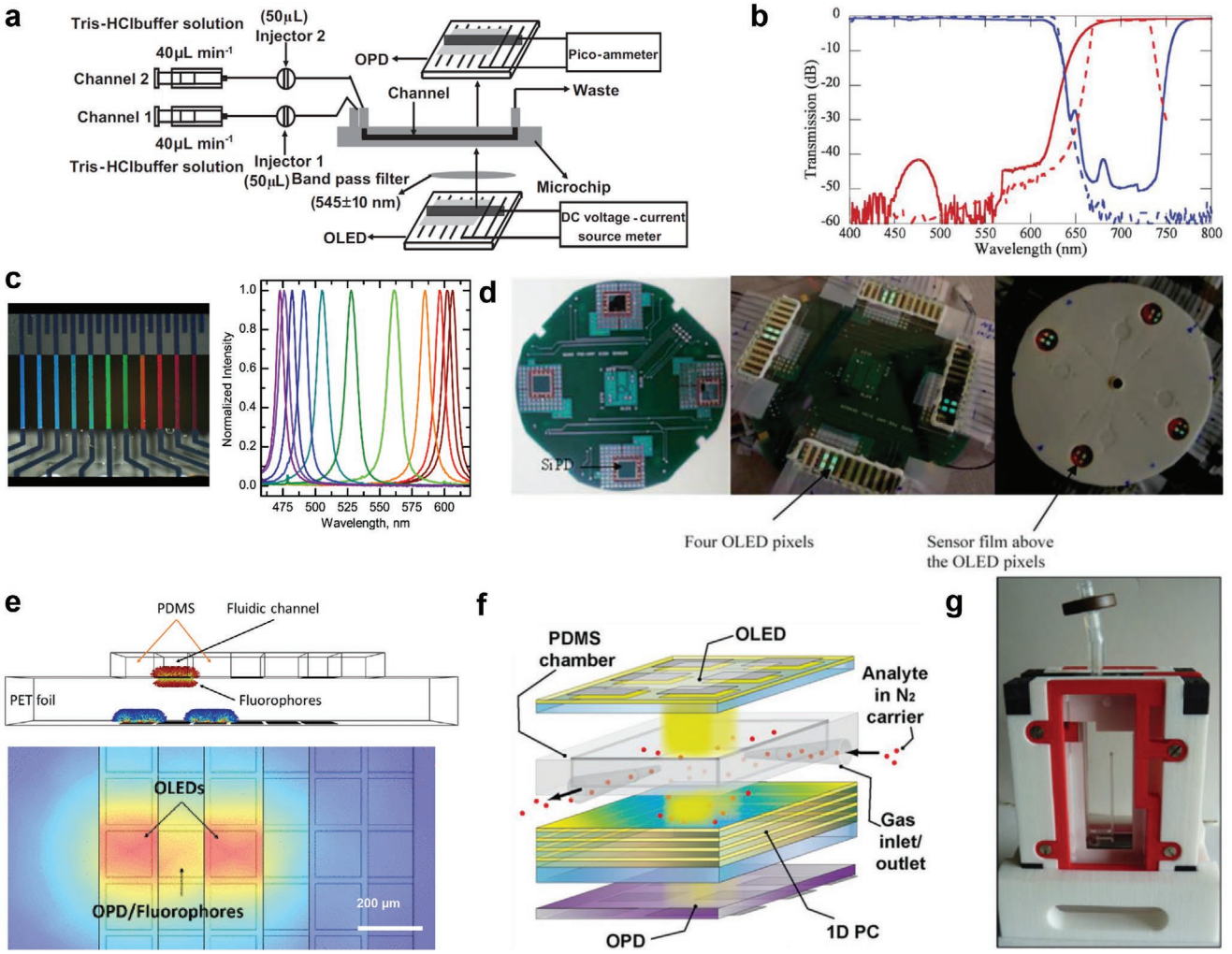

Figure 5. Application of OLEDs in microfluidic and lab-on-chip settings. a) Many examples of on-chip sensing use a sandwich-like configuration with a microfluidic device located between OLED light sources and silicon- or OPD-based light detectors. Reproduced with permission.[168] Copyright 2015, Elsevier. b) High-quality rejection of excitation light is essential for fluorescence detection. Carefully optimized absorption-based filters (solid lines) can provide an alternative to interference-based dielectric filters (dashed lines). Reproduced with permission.[171] Copyright 2012, The Royal Society of Chemistry. c) Combining white-emitting OLED stacks with microcavities of variable length allows on-chip generation of multicolor narrowband emission for spectroscopic studies. Reproduced with permission.[95] Copyright 2010, John Wiley and Sons. d) Using a rotating compact-disk layout, OLEDs and silicon photodiodes can be used to detect changes in the phosphorescence lifetime of Pt complexes. Reproduced with permission.[175] Copyright 2010, The Royal Society of Chemistry. e) Placing OPDs in a reflection configuration can reduce bleed-through of excitation light but requires close integration of OLEDs and OPDs. Reproduced under the terms and conditions of the CC-BY 4.0 license.[78] Copyright 2020, The Authors, published by IEEE. f) Changes in the resonance of a 1D photonic crystal are detected by an OLED/OPD pair, in the example shown to detect local concentration of alcohol vapor. Reproduced with permission.[196] Copyright 2014, John Wiley and Sons. g) OLEDs can also be used for plant cultivation in a photobioreactor. Reproduced with permission.[197] Copyright 2016, Elsevier.

unpolarized photoluminescence through a second polarizer that is oriented perpendicular to the first. Using this scheme in microfluidic devices that hold µL-scale sample volumes and that are sandwiched between an OLED and an OPD, rhodamine 6G and fluorescein can be detected at concentrations down to between 10^{-8} M and 10^{-5} M.[169,172,177] The use of lock-in detection can improve the robustness of the measurement to background fluctuations and can address the sub-linear nature of the fluorescence signal at low concentration.[166]

Rejecting excitation light through crossed polarizers is limited to nonscattering samples and devices because inelastic light-scattering can change polarization and will thus lead to excitation light reaching the detector. Spectral separation of excitation and fluorescence emission avoids this issue and is thus used more widely than the crossed polarizer approach. Spectral separation generally requires a long-pass or band-pass filter in front of the detector to block the shorter wavelength excitation light. In addition, as most emitter materials used in OLEDs show broad emission spectra with a long-wavelength emission tail, the excitation light usually also has to be conditioned by a filter. There are reports demonstrating such fluorescence detection schemes, combining OLED excitation with OPDs,[171,178] silicon detectors,[167,179] and direct visual detection.[178] Researchers have used absorption-based filters[171,178]

and dielectric interference-based filters[167,178,179] (Figure 5b). Interference filters generally show a sharper spectral response and higher rejection rates than absorption filters and are thus preferred in bench-scale optical systems such as fluorescence microscopes. However, their characteristics change strongly with the angle of incidence, which is problematic for compact devices where light is incident on the filters under a wide range of angles, i.e., the effective numerical aperture is large. Reducing the numerical aperture of the system through careful geometric optimization can partially solve this issue, but this comes at the cost of considerable light loss. If absorbing filters are used, it can be beneficial to perform the fluorescence detection on dyes with large Stokes shifts and to design the system such that the sensitivity of the OPD has minimal overlap with the OLED emission spectrum.[165]

An alternative strategy to reduce the leakage of excitation light to the detector is to design OLEDs with particularly narrow emission spectra. One way of achieving this is the use of emitter materials with intrinsically narrow emission,[163,168] such as TADF emitters based on the multiple resonance effect[180,181] or phosphorescent Pt-emitters with ligand centered emission.[182–184] Alternatively, one can integrate dielectric interference filters on the OLED, e.g., by depositing a distributed Bragg reflector (DBR) on top of a top-emitting OLED stack.[185] When doing this, special precautions have to be taken to avoid heat and/or radiation-induced degradation of the OLED during DBR deposition. We have recently reported strategies to manage this issue in pin-OLEDs, finding that both the n and the p contact of the device require special treatment.[186,187]

Another method to reduce the spectral width of the OLED emission, and at the same time tune the peak emission wavelength, is the integration of the OLED stack into an optical microcavity. By tuning the local thickness of the cavity across the substrate,[94] OLED pixels with narrowband emission across a wide range of the spectrum can be generated (Figures 3e and 5c).[95]

To avoid or reduce the reliance on filters on the detector side, tuning of the optical microcavity can also be used to narrow the excitation wavelength range in an OPD.[188] In the future, emerging photodetector materials may offer an even more efficient route to narrowing down the spectral range across which a photodetector is sensitive to light. Recently, thin-film perovskite-based photodetectors have shown promise in this context.[189–192] OLEDs and perovskite photodetectors have already been combined successfully for optocouplers and visible light communications.[193–195] Alternatively, one can replace the photodetector by a compact (fiber-coupled) spectrometer.[176] However, this comes at considerable additional cost, and stray light in the spectrometer may limit the quality of excitation rejection.

A further method to improve the contrast between excitation light and the photoluminescence signal is the use of time-gating. This has been employed in a system using a compact disk-shaped sample cartage with microfluidic channels embossed by ultrasound (Figure 5d).[175] Here the emission decay of a phosphorescent Pt-porphyrin dye with a luminescence decay time of 10s of μs is recorded to infer the concentration of glucose, lactate, ethanol, and dissolved oxygen in a sample.

Finally, the rejection of excitation light can also be improved by optimizing the detection geometry, e.g., changing from a transmission layout with OLED and detector sandwiching the sample cell to a reflection arrangement where the detector is arranged next to the OLED and the microfluidic channel with the analyte sitting on top of both (Figure 5e).[78] While this geometry can certainly be beneficial, in itself it did not suffice to allow detection of small concentrations of fluorescent dye.

In our view, the trade-offs between quality of excitation rejection, signal intensity, and other factors remain at least partially an unsolved challenge for lab-on-chip fluorescence detection. Further advances in this area are needed to fully capitalize on the benefits that fluorescence and the use of OLEDs can offer for lab-on-chip technology.

A potential route to avoid the challenges of fluorescence detection but still achieve higher sensitivity than absorption/transmission measurements, is the use of resonant photonic structures. For instance, a combination of OLED and OPD was used to read out shifts in the resonance of a photonic crystal upon exposure to alcohol vapor (Figure 5f).[196] This concept can likely be expanded to other analytes of interest. However, as such sensors fundamentally measure local change in refractive index, achieving specificity to the analyte of interest can be challenging.

While a lot of work on lab-on-chip devices has looked at proof-of-principle experiments by testing, e.g., the minimum concentration of a standard fluorescent dye that can be reliably detected, many groups have also worked on demonstrating the suitability of these devices in a range of applications. A particular focus has been on lateral flow devices,[164,178] immunosorbent assays, e.g., for immunoglobulin A (IgA),[167] and protein microarrays.[170,173] Another interesting application is a sensor that detects the fluorescence from chlorophyll in algae to assess the toxicity of herbicides and other water pollutants.[171] Somewhat different from this are proposals to integrate OLEDs in small-scale (plant) cultivation systems for high-throughput bioprocess development, where OLEDs effectively drive photosynthesis, e.g., of the algae *Chlamydomonas reinhardtii* (Figure 5g).[197]

In line with the promise of offering low-cost sensing capability, considerable effort has gone into developing simple and inexpensive manufacturing schemes for OLED-based lab-on-chip devices. In this context, solution processing is often seen as particularly attractive. In addition, in some cases, OLEDs have been replaced by organic electrochemical cells.[169,198]

3.2. OLEDs as Wearable Sensors for Health Monitoring

Wearable sensors have progressed significantly during the last decade: many people now wear smartwatches or activity trackers to record and monitor their health and fitness. While the optical sensors used in those devices consist of inorganic LEDs and photodiodes so far, organic LEDs and photodiodes are now explored for wearable sensing to enable higher flexibility and miniaturization and eventually achieve "imperceptible" sensors.

Important measures for personal health are the heart rate (pulse) and the oxygen content of the blood. Both can be measured optically by illuminating the skin and detecting

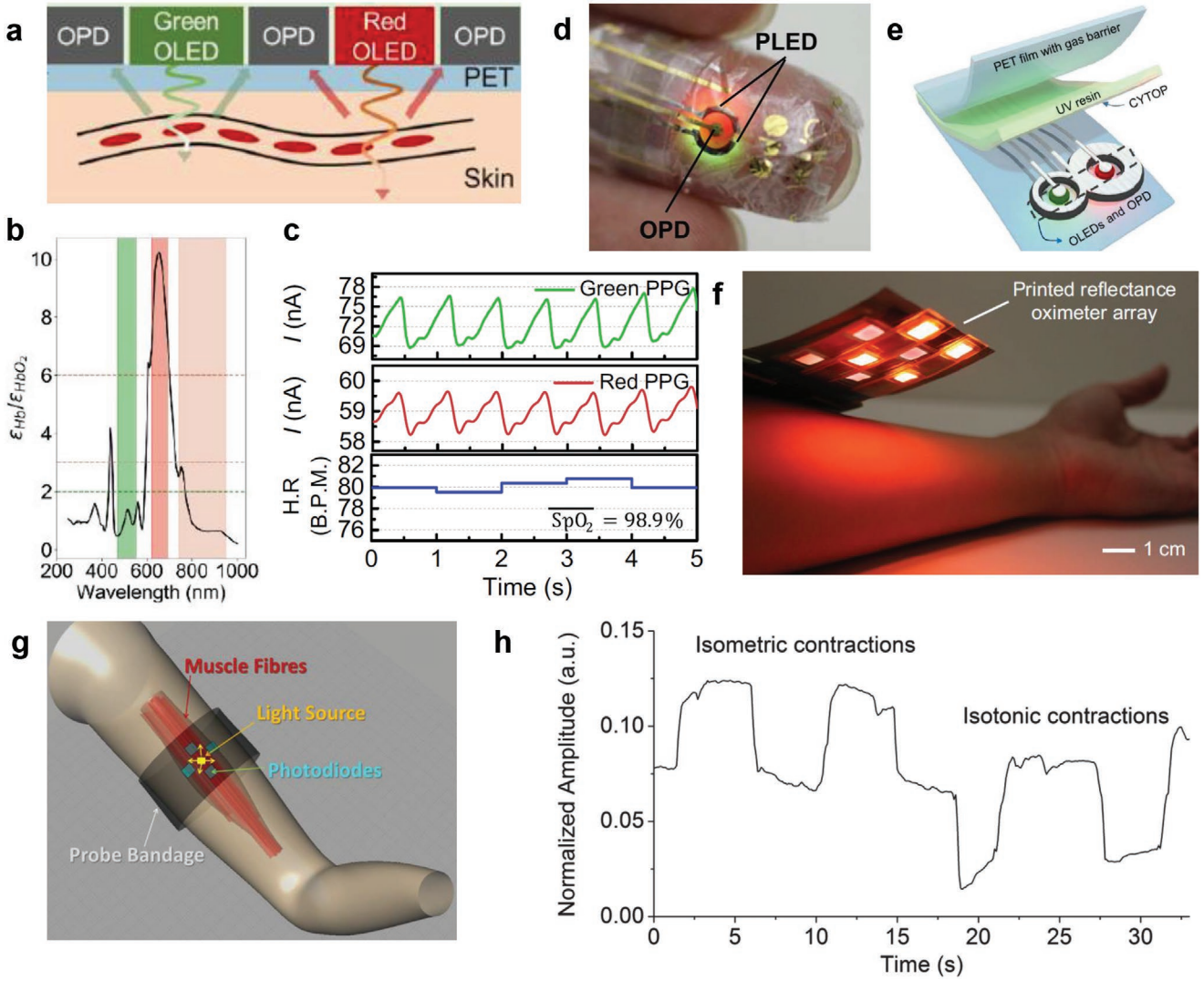

Figure 6. OLEDs for wearable sensors and health monitoring. a) The pulse rate is measured by detecting reflected light from blood vessels using OLEDs and OPDs. Reproduced with permission.[77] Copyright 2018, The Authors, published by AAAS. b) The measurement of oxygen saturation makes use of the different molar extinction ε of Hb and HbO_2 in the red spectral region. Reproduced with permission.[76] Copyright 2018, The Authors, published by National Academy of Sciences. c) Measuring the reflected light in the red and either green or infrared regime, it is possible to calculate SpO_2. Reproduced with permission.[77] Copyright 2018, The Authors, published by AAAS. d) Flexible pulse oximeter consisting of red/green polymer OLEDs and an OPD wrapped around a fingertip. Reproduced with permission.[52] Copyright 2016, The Authors, published by AAAS. e) Flexible oximeter with OLEDs and OPD integrated onto one substrate. Reproduced with permission.[77] Copyright 2018, The Authors, published by AAAS. f) Arranging several OLEDs and OPDs onto an array, it is possible to map oxygen saturation over larger areas. Reproduced with permission.[76] Copyright 2018, The Authors, published by National Academy of Sciences. g,h) OLEDs and OPDs can also be used to sense muscle contractions. Reproduced under the terms and conditions of the CC-BY license.[207] Copyright 2014, The Authors, published by Wiley-VCH.

either absorbed or reflected light with a photodiode sitting in transmission or reflection mode, respectively (**Figure 6**a). Red light is preferred due to its deeper penetration into tissue. The pulse is measured via photoplethysmography (PPG), which detects changes in the volume of the blood vessel. Saturation of peripheral oxygen (SpO_2) measures the percentage of oxygenated hemoglobin (HbO_2), which shows different absorption compared to deoxygenated hemoglobin (Hb) in the red spectral region (Figure 6b). By illuminating the skin at two different wavelengths using red and either green or infrared light, the oxygen saturation can be measured (Figure 6c). Since the measurement principle of both sensing techniques is the same, SpO_2-sensors can also be used to record PPG signals.[155]

PPG sensors based on polymer OLEDs and OPDs for emission and detection, respectively, were already demonstrated in 2008.[199,200] The Hattori group recently developed and characterized PPG sensors based on a red-emitting OLED using the phosphorescent emitter $Ir(piq)_3$ (peak wavelength: 625 nm) and an OPD containing a bulk heterojunction of DBP:C_{60}.[201–203] Through optimization of device geometry and OPD layer structure, detection with signal-to-noise ratio (SNR) of 54 dB was achieved at a low power consumption of 0.6 mW.[203] The authors also demonstrated a wireless device that required even

lower drive power but at the cost of reduced SNR.[202] Furthermore, they showed that the optimal design comprises a circular OLED surrounded by a ring-shaped photodiode. Though the opposite design (photodiode surrounded by OLED) can detect PPG signals at similar SNR, the power consumption of the system strongly depends on the size of the OLED meaning that significantly lower power consumption is achieved if the OLED is placed in the center.[201]

Pulse oximetry sensors based on OLEDs have hugely progressed in recent years. Lochner et al. developed the first SpO_2-sensor for quantitative analysis of oxygen saturation using rigid red and green polymer OLEDs in combination with a flexible PTB7:$PC_{71}BM$ polymer OPD.[204] They measured PPG and SpO_2 at the fingertip in transmission mode and achieved high accuracy with only 1% and 2% error for pulse rate and oxygenation level, respectively. Yokota et al. developed an ultraflexible pulse oximeter based on a substrate of alternating parylene/SiON layers with a total thickness of only 3 μm, red and green polymer OLEDs, and a P3HT:PCBM OPD (Figure 6d).[52] The devices were laminated onto the fingertip and pulse rate and SpO_2 were measured in reflection mode. Further development was achieved by Lee et al. who monolithically integrated phosphorescent red and green OLEDs and a small-molecule OPD on a flexible substrate (Figure 6e).[77] The authors studied light propagation in the skin as a function of OLED emission spectrum and used this to optimize the sensor layout. Interestingly, close contact between the device and the skin not only improves the signal by suppressing direct light emission from the OLED to the OPD but also increases the OLED outcoupling efficiency through improved index matching at the OLED/skin-interface.

A complete organic pulse oximeter was demonstrated by Lee et al., who integrated a red and green OLED and an OPD with silicon CMOS driver circuits and a battery onto a flexible, sticker-type substrate.[205] Patterning of OLEDs and sensors furthermore enabled spatially resolved measurements of tissue oxygenation over large areas. For this, Khan et al. developed a 2D blade-coated sensor array consisting of four red OLEDs (612 nm), four near-infrared OLEDs (725 nm), and eight OPDs for recording (Figure 6f).[76] The authors identified the forehead as ideal place to precisely measure oxygenation and also used the sensor to monitor the oxygen saturation on the forearm under pressure-induced ischemia. The mapping function of the sensor is highly promising for monitoring oxygen saturation of tissue, wounds, or organs postsurgery. Further development by Han et al. comprised parallel fabrication of red and green OLEDs for pulse oximeters via blade coating[80] and a pulse oximeter with OPDs working under ambient light conditions.[206]

Another sensor to record tissue oxygenation was developed by Bansal et al.[207] While this sensor consisted of only one OLED and hence did not allow quantitative calculation of HbO_2 concentration, the authors showed a further interesting application of an OLED-based optical sensor, namely to sense muscle contractions. The detection principle makes use of the fact that the intensity of light that is backscattered from skeletal muscle tissue depends on the orientation of the muscle fiber. By placing a solution-processed yellow-emitting OLED into the center of four surrounding OPDs (detection at 610–700 nm), one can differentiate between isotonic and isometric muscle contractions, which the authors ultimately used to operate a robotic arm (Figure 6g,h).

Finally, we note that light undergoes scattering and absorption in tissue, which not only leads to a reduction of the signal (with long wavelengths penetrating deeper into tissue) but as a result of the wavelength-dependent penetration depth also causes spectral broadening, with the strength of broadening increasing with increasing spectral width of the OLED electroluminescence.[208] Hence, on-skin applications requiring narrow spectra or bi-color excitation need to take this into consideration when designing OLEDs with suitable emission spectra.

3.3. OLEDs for Therapeutic Treatment

Besides the use of OLEDs for lab-on-chip applications and health monitoring, wearable OLEDs can also be used as light source for therapeutic treatment, which is particularly promising for outpatient care. Patch-type flexible OLEDs that can be integrated in plasters and worn directly on the skin show promise for point-of-care medical treatment. Two main applications were explored in the past: photodynamic therapy (PDT) and photobiomodulation (PBM).

PDT is a powerful method to treat cancer and kill bacteria, and has found application, e.g., in oncology, dermatology, ophthalmology, and dentistry. It requires light in a specific wavelength range to be delivered to a photosensitizer, which is administered either topically to the surface that needs treatment or systemically. The photosensitizer is a material with strong absorption and high intersystem crossing (ISC) rate to the triplet state. Upon excitation of the photosensitizer, triplet excitons interact with molecular oxygen present in the tissue, lifting oxygen from its triplet ground state into the singlet state. The created singlet oxygen species and free radicals are cytotoxic and thus attack nearby cells or bacteria (**Figure 7**a).[209] Interestingly, since a high ISC rate is crucial for efficient formation of singlet oxygen, the key principles used to design emitter materials that harvest triplet excitons in OLEDs also apply to the development of photosensitizers. This gave rise to new photosensitizers based on phosphorescent[210] and TADF[211–213] emitters.

So far, PDT relies on high power light sources such as LEDs and lasers to deliver light to the targeted area. The activation wavelength of most photosensitizers lies in the red wavelength regime, between 600 and 750 nm. Red light is preferred due to its enhanced penetration through the skin, with key requirement being that the wavelength is below 800 nm to provide enough energy to excite singlet oxygen.[214] Traditionally, in PDT light is delivered with a power density (fluence rate) of around 1 mW mm^{-2} and doses of around 50–100 J cm^{-2}. However, there is evidence that light delivery at lower powers is less painful.[215] In order to achieve the same dose at lower power, longer treatment is required, which renders light sources that can be worn over several hours particularly attractive.

In a clinical study, Attili et al. used a wearable red OLED delivering 0.05 mW mm^{-2} at a peak wavelength of 620 nm to treat nonmelanoma skin cancer (Figure 7b).[216] Patients scored the pain experienced during treatment as significantly lower

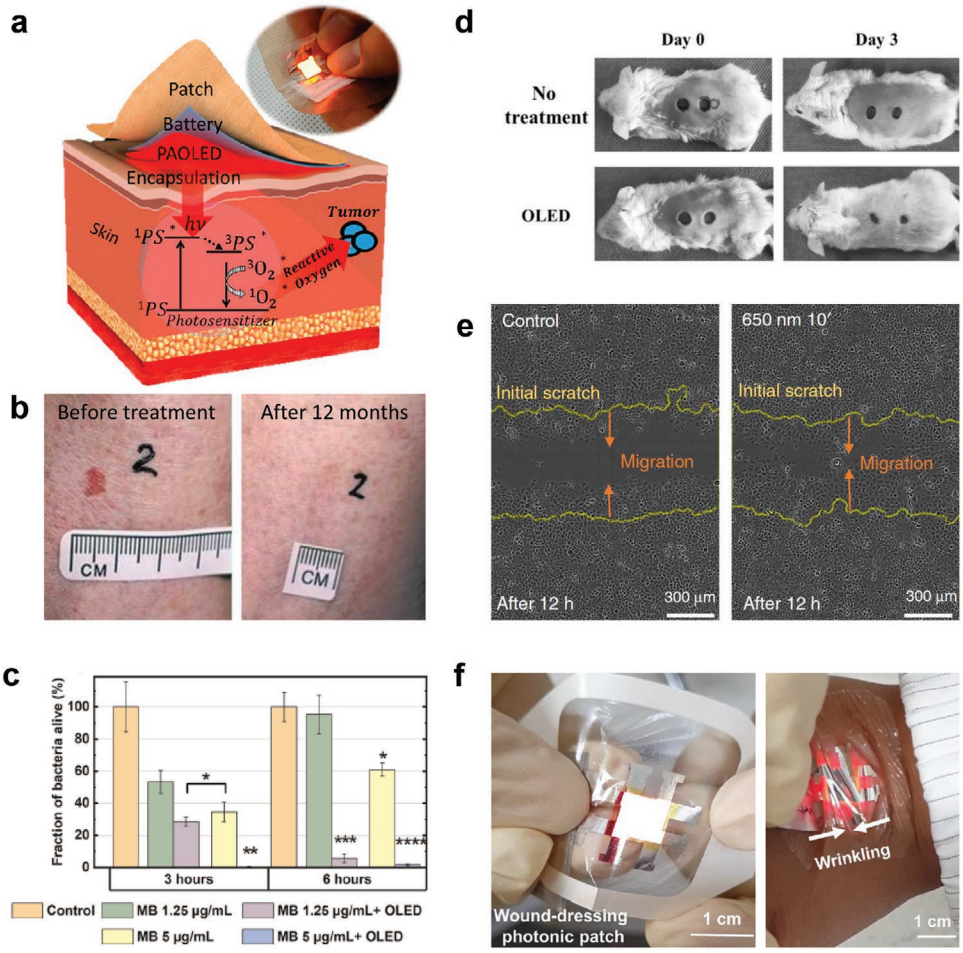

Figure 7. OLEDs for therapeutic treatment. a) Wearable OLED patches can be attached to the skin to treat cancer. PDT uses light to excite a photosensitizer, which subsequently transfers its energy to oxygen forming reactive singlet oxygen. This can attack nearby cells. Reproduced with permission.[144] Copyright 2020, American Chemical Society. b) Successful treatment of skin cancer via PDT using a red-emitting OLED. Reproduced with permission.[216] Copyright 2009, John Wiley and Sons. c) Antimicrobial PDT using flexible OLEDs and the photosensitizer methylene blue (MB). Reproduced under the terms and conditions of the CC-BY 4.0 license.[218] Copyright 2019, The Authors, published by Springer Nature. d) Accelerated wound healing in mice via PBM under OLED illumination. Reproduced with permission.[222] Copyright 2019, The Authors, published by Korea Institute of Science and Technology Information. e) Improved migration of keratinocyte cells in vitro under 650 nm illumination with an OLED. Reproduced under the terms and conditions of the CC-BY 4.0 license.[73] Copyright 2019, The Authors, published by Springer Nature. f) Flexible, 6 μm thin OLED attached to a transparent wound dressing film. Reproduced with permission.[224] Copyright 2020, Wiley-VCH.

when the OLED was used, compared to a control group that was treated with an inorganic LED delivering a similar dose but at a higher fluence of 0.75 mW mm^{-2}. The successful treatment of cancer using OLEDs at low fluence was further supported in an animal study that delivered 0.03 mW mm^{-2} to treat glioma in mice.[217] In both studies, rigid OLEDs with glass substrates were used, which restricts the comfort when worn a long time. Recently, flexible high-power OLEDs achieving up to 1 mW mm^{-2} below 8 V were developed by connecting two stacked red-emitting devices in parallel (Figures 4d,e and 7a).[144] Using these devices for in vitro PDT the authors showed a significant reduction in the viability of mouse melanoma cells at 0.35 mW mm^{-2}. Another study demonstrated the potential of antimicrobial PDT with flexible OLEDs as an alternative to antibiotics. Here, Lian et al. developed top-emitting red OLEDs and showed the killing of *Staphylococcus aureus* after light application for 6 h at 0.06 mW mm^{-2} (Figure 7c).[218]

PBM describes the use of low-intensity light for therapy, e.g., to accelerate wound healing, to reduce inflammation, or relieve pain. The underlying mechanisms depend on the type of therapy, the cell type treated, and the molecular processes involved, and in a significant fraction of cases are not fully understood.[219] The most accepted theory suggests that light absorption leads to improved production of adenosine triphosphate (ATP) in mitochondria and thus improved energy delivery to regulate cellular processes.[220]

The use of OLEDs for PBM was first explored with the aim to accelerate wound healing of diabetic models in vitro and in vivo.[221] For this, top-emitting OLEDs based on the phosphorescent emitter Ir(piq)$_2$(acac) with a peak wavelength of 623 nm were used. The devices were operated at 0.1 mW mm^{-2} and—incorporating a conventional heat-sink with a fin structure—constant operation at this power density led to a surface temperature of 39.6 °C, sufficiently low for on-skin application.

Results on a diabetic model of human dermal fibroblasts showed increased ATP formation and enhanced cell proliferation when doses of 0.2 and 1 J cm^{-2} were delivered by the OLED. Further evidence was shown in diabetic rats, where both OLED and laser treatment of wounds led to accelerated wound closure after 5 d postsurgery at a dose of 5 J cm^{-2} (around 8 min of daily operation).[221] Similar results were also found in (non-diabetic) mouse models, where OLEDs and LEDs with a peak wavelength of 633 nm were used to accelerate wound healing and to promote collagen regeneration at 0.05 mW mm^{-2}, administered in daily doses of 6 J cm^{-2} (Figure 7d).[222]

Jeon et al. developed a wearable OLED patch, fully integrated with a flexible battery and thin-film encapsulation.[223] The emission color was adjusted to peak wavelengths between 609 and 690 nm by changing the thickness of the OLED microcavity. Applying a 75 μm thin graphite heat sink, the operation temperature at the surface was maintained to below 40 °C after 20 minutes of operation at 0.18 mW mm^{-2}. The authors studied the effect of OLED illumination on human fibroblast cells in vitro and found significant enhancement of cell proliferation and migration at all wavelengths when driving the OLEDs at 0.05 mW mm^{-2} with doses of 3 to 9 J cm^{-2}. Later, they performed a similar in vitro study on keratinocytes and found best results for illumination at 670 nm wavelength (Figure 7e).[73] Furthermore, they confirmed rapid wound healing in a wounded rat skin model, where re-epithelialization was induced,[73] and in a 3D artificial skin model consisting of both dermis and epidermis.[224] The flexibility and possibility to attach to different surfaces including commercial wound dressing films make the OLEDs highly promising as wearable light sources for medical treatment (Figure 7f).

Besides PDT and PBM, the use of OLEDs was also explored in a clinical study that investigated the safety and acceptability of light therapy for retinal diseases. Here, green OLEDs (peak wavelength: 504 nm, luminance: 80 cd m^{-2}) matching the scotopic response of the human eye were incorporated into sleep masks to suppress dark adaptation.[225] Another study compared ophthalmic toxicity effects between white OLEDs and LEDs and found reduced toxicity for OLEDs.[226] This was explained by the reduced blue-wavelength component in the OLED emission spectrum.

3.4. OLEDs for Optogenetics

Another emerging field of application for OLEDs is the optical stimulation of cells through a technique called optogenetics. First demonstrated in 2005 by Boyden et al.,[227] optogenetics genetically programs cells to produce light-sensitive proteins, in many cases light-gated ion channels or light-gated ion pumps. This in turn can confer light sensitivity to the genetically modified cells themselves (**Figure 8**a). Optogenetics is particularly promising for precisely timed control of neuronal activity with very high spatial resolution and allows both activation and inhibition of cellular activity. It is now an established technique in neuroscience that has enabled a number of breakthrough findings in behavioral biology,[228,229] revealed important insight into neurological diseases such as Alzheimer's or Parkinson's disease,[230–232] and led to the inventions of optical pacemakers,[233,234] devices for optical bladder control,[235] and many others. It may soon find application in the clinic, where it may help restore or aid vision and hearing for visually and hearing-impaired patients.[236–239]

Most typically, LEDs and lasers are used for light delivery in optogenetics, both in vitro and in vivo.[240] While these light sources provide high power and good spectral control, they are generally rigid and provide only relatively low spatial resolution. OLEDs instead can be patterned into pixels that are as small as individual cells, which corresponds to a display resolution of more than 2500 ppi.[97,241] Furthermore, they can be mechanically flexible and water-resistant,[74] transparent,[242,243] and designed to enable dynamic switching of the emitted color.[244] These features make OLEDs highly attractive as functional implants in animal studies, where they may enable rapid addressing of individual target cells or clusters of cells, could be used for bicolor optogenetics, and may even provide the excitation light for simultaneous optical readout. At the same time, flexible OLEDs will help to reduce the inflammatory tissue response that is often observed due to mechanical mismatch of rigid implants with soft tissue.[245]

The emission spectrum of any light source used for optogenetics should show good overlap with the absorption spectrum of the light-sensitive protein used. To encode the expression of light-gated ion channels or pumps, microbial opsin proteins are frequently used, with channelrhodopsin-2 (ChR2) and mutations of ChR2 probably being the most common. ChR2 is most sensitive in the blue spectral region but in the past 15 years many variants have been engineered that enable response across the whole visible range. Early versions of ChRs required optical power densities well above 1 mW mm^{-2}, but nowadays modified opsin proteins such as CsChrimson and $ChR2^{XXL}$ respond to light levels below 10 μW mm^{-2} (Figure 8b).[246,247] The power density required to achieve robust optical stimulation of cells in a specific experiment will likely depend on the opsin expression level. In addition, higher power levels may be needed for the stimulation of individual neurons in culture compared to animal studies or clinical use in implants where the connected nature of the tissue will typically trigger multiple neurons simultaneously. Nevertheless, depending on the specific application, the power density requirements of optogenetics may require the use of highly optimized and adapted OLED architectures.

Using a blue-emitting OLED microdisplay providing a surface power density of 1 μW mm^{-2}, Steude et al. demonstrated that the movement of *Chlamydomonas reinhardtii*, a type of unicellular algae cells that naturally expresses ChR2, can be controlled via local light-stimulation from the display.[248] The OLEDs were capped by a multilayer TFE consisting of aluminum oxide and a crosslinked acrylic polymer, which enabled stable device performance in water and physiological solutions for three days. In a second study, the authors used an OLED microdisplay to optically control the membrane current in a mammalian cell line (HEK cells) genetically modified to produce a ChR2 mutant (Figure 8c–e).[249] The study found high cell viability and good adhesion of cells when the TFE was coated with poly-L-lysine and fibronectin. In patch-clamp experiments, HEK-cells transfected with ChR2-H134R and ChR2-C128S/D156A showed robust photostimulation under

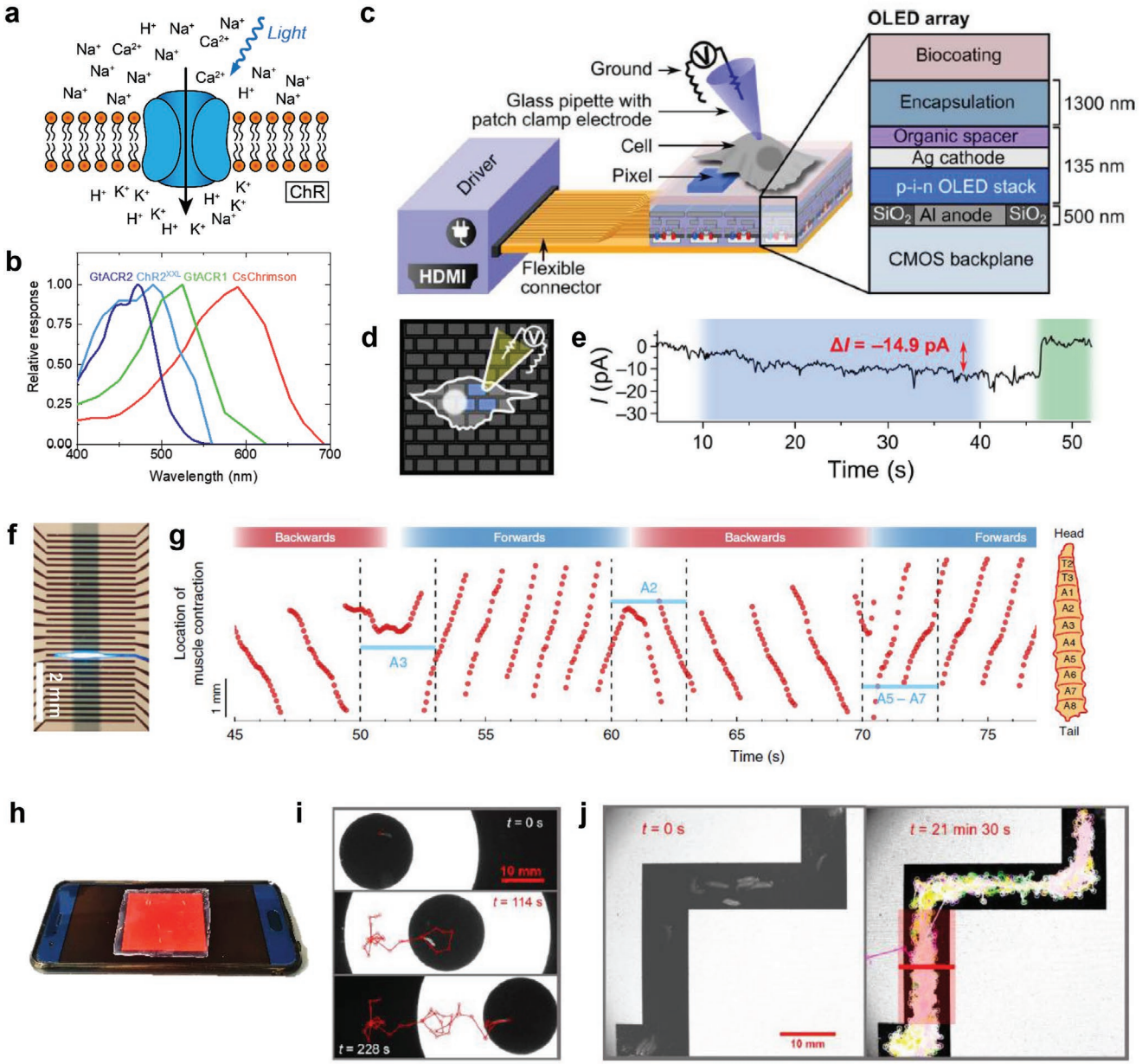

Figure 8. Patterned OLEDs for optogenetics. a) Optogenetics introduces light-sensitive ion channels into the cell membrane that regulate the flux of ions in response to light. b) Activation spectra of common light-sensitive activators and inhibitors. Reproduced under the terms and conditions of the CC-BY 4.0 license.[251] Copyright 2020, The Authors, published by Springer Nature. c) Structure of an OLED microdisplay used for optogenetic stimulation of HEK-cells. d,e) Schematic of a cell stimulated by the microdisplay and current *I* across the cell membrane during 30 s of OLED photostimulation. c–e) Reproduced with permission.[249] Copyright 2016, The Authors, published by AAAS. f) Lithographically structured OLED used for segment-specific stimulation of *Drosophila* larvae. g) Switching of the larval crawling direction upon targeted sensory photostimulation of neurons in individual segments. f,g) Reproduced under the terms and conditions of the CC-BY 4.0 license.[79] Copyright 2020, The Authors, published by Springer Nature. h) Schematic illustration of optogenetic stimulation of *Drosophila* larvae using smartphone displays. i) A larva guided on the display by moving a ring of light. Red lines show larval trajectory. j) Larvae constrained inside a maze of light displayed by the smartphone display. Left: Position of larvae at start of experiment; right: trajectories of larval crawling after 21 min. h–j) Reproduced under the terms and conditions of the CC-BY 4.0 license.[251] Copyright 2020, The Authors, published by Springer Nature.

OLED illumination. The authors furthermore demonstrated the high-resolution capability of the display by showing that cells only responded to stimulation from OLED-pixels immediately underneath the cell, but not to stimulation from close-by pixels. The light intensity provided by these early microdisplays, however, was at the lower limit of what would be required to enable stimulation in neuronal cultures.

The first direct evidence that OLEDs can stimulate neurons was given by Morton et al., who developed blue, green, and red OLEDs to stimulate opsin-expressing motor neurons

in *Drosophila melanogaster* (fruit fly) larvae.[250] The OLEDs contained doped charge transport layers and achieved light intensities of 0.25 to 0.4 mW mm^{-2} at a driving voltage of 5 V. The authors demonstrated successful neuronal activation with blue and green OLEDs and showed that as expected the spectral overlap of the red OLED emission and the opsin used was insufficient to trigger a motor neuron response. We developed microstructured, top-emitting blue OLEDs with pixel widths of 100 µm to stimulate sensory neurons in individual abdominal segments of *Drosophila* larvae (Figure 8f,g).[79] The OLEDs were used for both activation and inhibition of neuronal activity using the ChRs CsChrimson and GtACR2, which elicited response to light intensities from 2 and 8 µW mm^{-2} onwards, respectively. Targeted stimulation of neurons in anterior and posterior segments of the larvae triggered crawling waves and switches in the direction of crawling, demonstrating the value of patterned OLEDs to deliver light at high spatial resolution for improved targeting of neurons. Recently, Meloni et al. showed that *Drosophila* larvae expressing highly light-sensitive ChRs can even be stimulated by conventional smartphones (with OLED and LCD displays), which emit light at intensities of 0.8 to 2.8 µW mm^{-2} per RGB sub-pixel.[251] The authors developed an Android-based app and showed that this can be used to constrain and guide larvae by displaying suitable light patterns (Figure 8h–j).

OLEDs were also used to stimulate neurons in culture, even though this required significantly higher light intensities. Morton et al. used blue-emitting small-molecule OLEDs to excite primary mouse hippocampal neurons expressing CheRiff, a blue-responsive ChR (**Figure 9**a–c).[150] Simultaneously, the cells were coexpressing a red-emitting calcium indicator, jRCaMP1a, which was used to read out neuronal activity. This approach enabled all-optical and noncontact mapping of neuronal activity. Cellular response was observed for light intensities from ≈60 µW mm^{-2} (corresponding to an OLED drive current of 63 mA cm^{-2} at a voltage of 3.4 V) and increased as the OLED drive current was further increased (Figure 9c). According to established protocols in optogenetics, OLEDs were operated with a series of 10 ms long pulses, which also helped to reduce thermal stress to the OLEDs when they were driven at high intensity. At an initial power density of 0.5 mW mm^{-2}, the OLEDs showed relatively slow degradation with only 20% loss in light intensity after one million stimulation pulses of 10 ms length at 10 Hz.

A pulsed driving mode for stimulation of cultured primary hippocampal neurons was also used in recent work by Matarèse et al.[151] The authors developed solution-processed blue and orange OLEDs to stimulate either the bi-stable ChR2-C128S/D156A or ChrimsonR (Figure 9d,e). Firing of action potentials from neurons in response to OLED stimulation was recorded by patch-clamp electrophysiology. For ChrimsonR-expressing neurons, the firing rate was controlled by delivering 50 ms long pulses with light intensities of 150 µW mm^{-2} by driving the OLED at 30 V with 10 kHz pulses. Furthermore, the authors measured the temperature rise of their OLEDs when driven either in DC mode or with square-wave pulses of 10 kHz and 50 % duty cycle and found an increase of 1.1 °C and 0.7 °C, respectively, after 3 s drive (Figure 9f). Typically, temperature increases of up to 1°C are considered safe for most cells in culture and in vivo. Since the OLEDs used in this work showed an EQE of less than 0.5 % and were driven at 30 V, it is expected that OLEDs with higher EQE and lower drive voltages will pose even lower thermal stress to adjacent cells. In addition, for in vivo applications, blood flow in the tissue will improve heat dissipation compared to experiments in culture.

Recently, Kim et al. developed ultraflexible, 2 µm thin OLEDs and used those to control motor and sensory neurons in rats expressing ChR2 (Figure 9g,h).[49] Under application of 5 ms long light pulses at 15 V, the OLED generated more than 0.5 mW mm^{-2} of optical intensity, which allowed control of hindlimb movement and contraction of the gastrocnemius muscle by targeted nerve stimulation. The authors studied the mechanical damage at the sciatic nerve when implanting a flexible OLED and compared this to the damage caused by a cuff representing a rigid light source. Histological examination of the nerve tissue after 10 d revealed that, in contrast to the rigid cuff, the OLED posed no significant stress to the nerve due to its high mechanical flexibility. Furthermore, the authors showed that OLEDs can be used for simultaneous neuroimaging via MRI, which is a significant advantage over inorganic and metallic devices since those introduce image artifacts in MRI due to their magnetic response (Figure 9i). Optogenetic stimulation of cortical neurons in culture and in vivo was also investigated by Sridharan et al. using simultaneous read-out of neuronal activity via microelectrode arrays.[252] For this, blue and green OLEDs on PET substrates were used, which reached power densities exceeding 1 mW mm^{-2} when driven in pulsed mode at 10 Hz/10 ms at voltages of 12.5 V (blue OLEDs) and 15 V (green OLEDs).

While optical stimulation of neurons is highly promising both for basic neuroscience research and for clinical application, often neuronal activity needs to be recorded simultaneously. Optical reporters can respond to, e.g., the calcium concentration in the cell or the voltage across the cell membrane through changes in fluorescence quantum yield and thus enable a live read-out of neuronal activity and at cellular or in some cases even sub-cellular resolution. Morton et al. used such an all-optical approach employing a genetically encoded calcium indicator (GECI) to validate optogenetic stimulation of primary neurons by an OLED (Figure 9a–c).[150] A time-gated detection approach was used to avoid crosstalk between the relatively broad emission spectrum of the OLED used for optogenetic excitation and the much weaker fluorescence from the calcium indicator.

In order to make OLEDs also useful as an excitation source for fluorescence imaging, we narrowed the spectrum of a blue-emitting OLED by attaching a DBR (**Figure 10**a).[179] Depending on the numerical aperture of the objective, we reached image contrasts of more than 100:1 when exciting the green-emitting dye PM556 with this OLED configuration. We then demonstrated that OLEDs can be used for fluorescence imaging of GFP-expressing live cells in culture (Figure 10b) and muscles in *Drosophila melanogaster* larvae. Additionally, neuronal activity was detected by using an OLED to excite the GECI GCaMP6s expressed in the central nervous system of a *Drosophila* larva (Figure 10c).

Using OLEDs to excite fluorescence and thus detect cellular activity is particularly appealing due to the possibility to include OPDs for detection on the same, potentially flexible substrate. Rezaei-Mazinani et al. developed OPDs for monitoring of

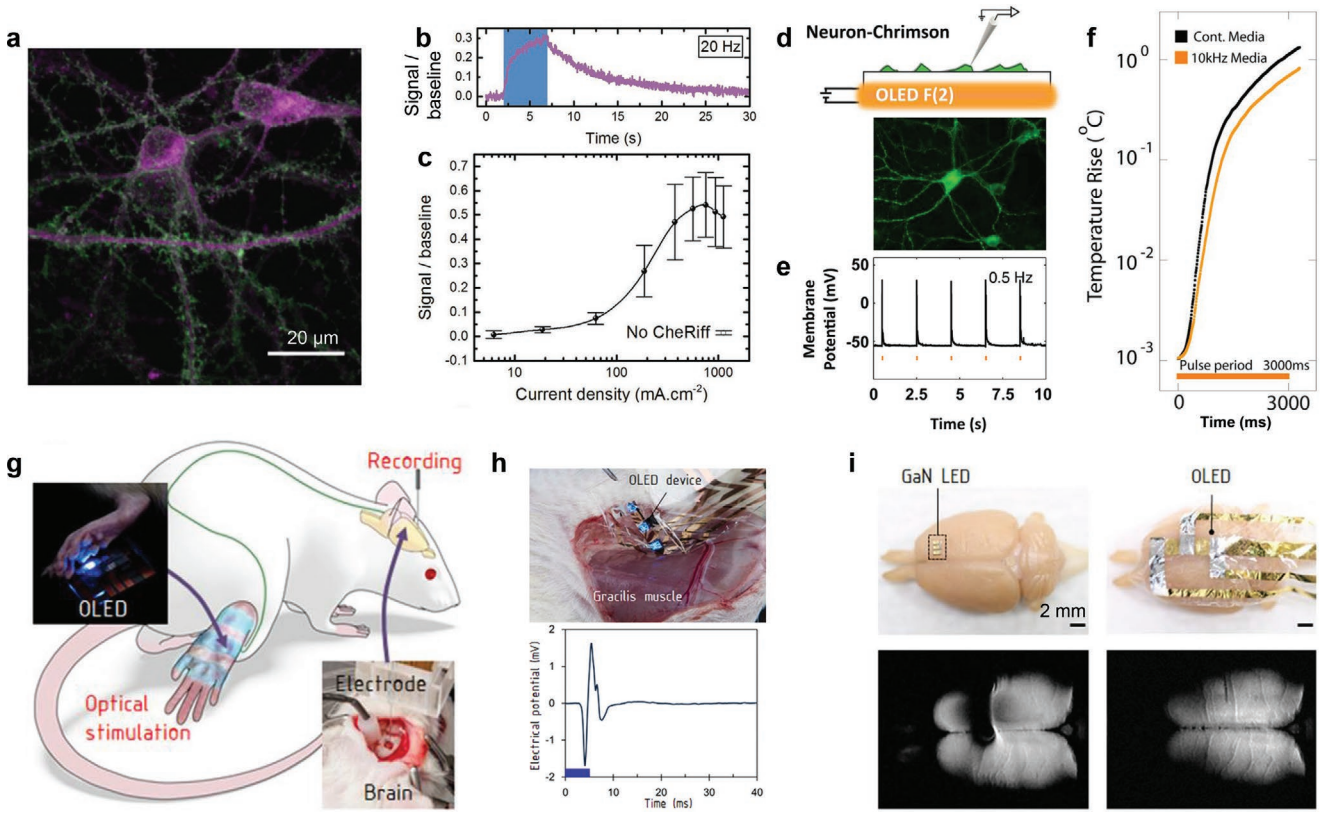

Figure 9. Optogenetics for neuronal activation in vitro and in vivo. a–c) All-optical optogenetics using OLED excitation and optical read-out. a) Hippocampal neurons expressing CheRiff-eGFP (green) and jRCaMP1a (magenta). b,c) Neuronal response upon optogenetic stimulation with an OLED as a function of time and OLED drive current density. a–c) Reproduced under the terms and conditions of the CC-BY 4.0 license.[150] Copyright 2019, The Authors, published by Wiley-VCH. d–f) Millisecond control of neuronal firing using orange-emitting OLEDs and the ChR ChrimsonR expressed in primary hippocampal neurons. e) The membrane potential shows firing of action potentials after stimulation with 50 ms pulses. f) Temperature rise upon driving the OLED in DC and pulsed mode. d–f) Reproduced under the terms and conditions of the CC-BY 4.0 license.[151] Copyright 2019, The Authors, published by Frontiers. g–i) Ultraflexible OLEDs used for stimulation of sensory neurons in rats. h) OLED attached to the gracilis muscle and electrical potential evoked by OLED stimulation. i) Photographs and MRI scans of perfused rat brains with attached GaN LED and OLED, respectively. Artifacts in the MRI scan are only visible for the GaN LED. g–i) Reproduced with permission.[49] Copyright 2020, National Academy of Sciences.

intrinsic optical brain signals[253] and of neuronal activity using calcium-sensitive dyes and the genetically encoded calcium indicator GCaMP6f (Figure 10d–f).[254] The solution-processed OPDs showed high detectivity, a wide linear response at low light intensities, sufficient temporal resolution in the millisecond range, and very low dark current at physiological temperatures. Although these experiments were done by collecting calcium signals underneath a microscope and without spatially resolving the signal, the potential of using OPDs was clearly demonstrated. Very recently, Kielar et al. achieved recording of neuronal activity from the fluorescent calcium indicator Cal-520 using OPDs with an absorber layer of rubrene/C_{60}.[255] The authors demonstrated detection of light intensities as low as 2.3 nW cm^{-2} when using magnifying optics underneath a microscope and they further demonstrated successful neuronal recording also when the device was placed underneath the cells. With the possibility to pattern OLEDs and OPDs into small pixels and to integrate both onto a flexible substrate, we expect that organic devices may ultimately allow high-resolution neuronal control with simultaneous mapping of activity in free-roaming animals.

4. Discussion and Conclusions

In conclusion, OLEDs have a number of unique characteristics that render them highly relevant for biomedical applications. Of particular note in this context is the inherent mechanical flexibility of organic semiconductors. While making robust and durable flexible OLEDs remains challenging, this possibility renders OLEDs ideally suited for applications that require close interfacing of the device to skin or tissue, or the integration of the OLED with another device of complex shape.

Researchers have demonstrated the benefits of OLEDs for biomedical applications in many feasibility tests and proof-of-concept studies. There are now already a small number of examples where OLEDs begin to be used outside the labs of organic electronics experts, for example in neuroscience research. Basic research in biology and medicine is a sensible intermediate step in developing OLEDs for future applications in human health. It provides a valuable proving ground for the technology as it entails many of the challenges that will be encountered in medical settings, but with fewer risks and regulatory hurdles.

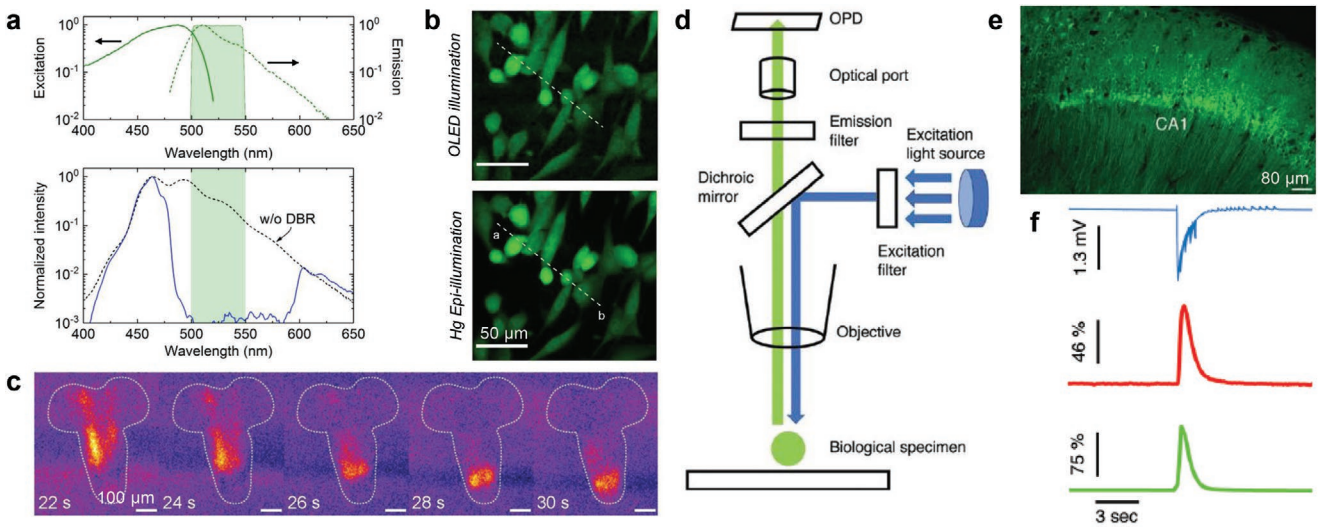

Figure 10. OLEDs and OPDs for imaging of neuronal activity. a) Emission and excitation spectrum of eGFP (top) and OLED emission spectrum in forward direction with (blue, solid line) and without (dashed line) DBR (bottom). b) Fluorescence intensity of live fibroblasts with cytoplasmic expression of eGFP under excitation with an OLED (top) and a conventional mercury light source (bottom). c) Calcium imaging of *Drosophila* larval CNS under OLED illumination. Heat maps show changes in larval activity over time indicative of fictive crawling activity. a–c) Reproduced and adapted with permission.[179] Copyright 2019, John Wiley and Sons. d–f) Recording neuronal activity by an OPD. d) Experimental setup. e) Expression of GCaMP6f in a hippocampal slice. f) Electrical stimulus of neuronal activity (blue), optical recording of Ca signal using OPD (red) and a CCD camera (green). d–f) Reproduced with permission.[254] Copyright 2019, The Royal Society of Chemistry.

In this review, we focused on the OLED aspect of the devices we discussed. In many cases, however, the devices also contain OPDs for light detection. For more information on the state-of-the-art in OPDs, we refer the reader to refs. [256–258]. Beyond OLEDs, other organic electronic devices are already used quite widely in the biomedical community, e.g., scientists have developed organic electrodes, photoactive organic substrates, and organic field effect transistors (OFETs, and in particular electrolyte-gated OFETs) to stimulate and sense electrical potentials in brain tissue, the peripheral nervous system and in muscle tissue. These efforts have been reviewed in refs. [259–262]. Compared to this work, the use of OLEDs in biomedical applications is less advanced. We attribute this to the more recent prominence of biophotonics as a whole, to the more stringent encapsulation requirements for OLEDs than for many other organic electronic devices, and the fact that OLEDs with the performance and stability required for many biomedical applications have only become available rather recently.

Moving forward, besides the potential to make mechanically flexible devices, key advantages of OLEDs for biomedical use are their ability to be deposited directly on a variety of substrates and to be made in various different sizes. In fact, these features are among the main reasons that OLEDs (and not inorganic LEDs) have become the technology of choice for self-emissive displays, from smartphones to TVs. For sensors and bioimplantable devices, rather than depositing OLEDs on large thin-film-transistor backplanes as done for displays, it may be more attractive to deposit them directly on silicon-based ICs. In many regards this monolithic integration of organic semiconductors on silicon combines the "best of both worlds": it offers the ability to integrate data-processing, driver electronics, and even photodetectors in silicon, and deals with the non-emissive nature of silicon without requiring the complex and error-prone flip-chip bonding or pick-and-place assembly routines that are required for the integration of inorganic LEDs. However, the integration of OLEDs on silicon ICs renders it more difficult to obtain mechanically flexible devices even though extreme thinning of silicon allows to achieve a degree of mechanical flexibility. Integration of OLEDs on silicon is already used to make OLED microdisplays,[93,263–265] some of which are bidirectional, e.g., to combine eye tracking and display function in optical viewfinders and smart glasses.[266]

At the same time, this design flexibility of OLEDs represents challenges for the wider uptake of OLEDs in terms of system integration and manufacturing. Today, the manufacture of silicon ICs and to a lesser extent also of integrated photonics happens mostly in so called foundries, i.e., large semiconductor fabrication plants. Foundries use a set of standardized fabrication processes to rapidly manufacture large numbers of devices with custom designs and bespoke functionality. By contrast, at least for now, OLED-based devices are produced in more specialized facilities, namely in large display fabrication plants and in a number of much smaller pilot production lines and research labs. With the high level of maturity that OLEDs have now reached, it will be interesting to see if the industry decides to introduce some standard OLED stacks as a routine foundry process. This would open up vast opportunities for small-scale production of OLED-based devices with custom designs and would thus enable a range of applications from on-chip sensing to wearable electronics.

Acknowledgements

This research was financially supported by the EPSRC NSF-CBET lead agency agreement (EP/R010595/1, 1706207) and the Leverhulme Trust

(RPG-2017-231). M.C.G. acknowledges support from the Alexander von Humboldt-Stiftung through the Humboldt-Professorship. Diese Arbeit wurde mitfinanziert durch Steuermittel auf der Grundlage des vom Sächsischen Landtag beschlossenen Haushaltes.

Conflict of Interest

The authors declare no conflict of interest.

Keywords

biointegrated electronics, biophotonics, organic LEDs, photomedicine, transient electronics

Received: February 5, 2021
Revised: March 12, 2021
Published online:

[1] S. H. Yun, S. J. J. Kwok, *Nat. Biomed. Eng.* **2017**, *1*, 0008.
[2] K. Goda, *APL Photonics* **2019**, *4*, 050401.
[3] C. Krafft, *J. Biophotonics* **2016**, *9*, 1362.
[4] G.-H. Lee, H. Moon, H. Kim, G. H. Lee, W. Kwon, S. Yoo, D. Myung, S. H. Yun, Z. Bao, S. K. Hahn, *Nat. Rev. Mater.* **2020**, *5*, 149.
[5] C. W. Tang, S. A. VanSlyke, *Appl. Phys. Lett.* **1987**, *51*, 913.
[6] J. H. Burroughes, D. D. C. Bradley, A. R. Brown, R. N. Marks, K. Mackay, R. H. Friend, P. L. Burns, A. B. Holmes, *Nature* **1990**, *347*, 539.
[7] Z. Yang, Z. Mao, Z. Xie, Y. Zhang, S. Liu, J. Zhao, J. Xu, Z. Chi, M. P. Aldred, *Chem. Soc. Rev.* **2017**, *46*, 915.
[8] Y. Liu, C. Li, Z. Ren, S. Yan, M. R. Bryce, *Nat. Rev. Mater.* **2018**, *3*, 18020.
[9] K.-H. Kim, J. Kim, *Adv. Mater.* **2018**, *30*, 1705600.
[10] S. Ho, S. Liu, Y. Chen, F. So, *J. Photonics Energy* **2015**, *5*, 057611.
[11] J. Blochwitz, M. Pfeiffer, T. Fritz, K. Leo, *Appl. Phys. Lett.* **1998**, *73*, 729.
[12] G. He, M. Pfeiffer, K. Leo, M. Hofmann, J. Birnstock, R. Pudzich, J. Salbeck, *Appl. Phys. Lett.* **2004**, *85*, 3911.
[13] K. Walzer, B. Maennig, M. Pfeiffer, K. Leo, *Chem. Rev.* **2007**, *107*, 1233.
[14] G. Schwartz, S. Reineke, T. C. Rosenow, K. Walzer, K. Leo, *Adv. Funct. Mater.* **2009**, *19*, 1319.
[15] S. Reineke, F. Lindner, G. Schwartz, N. Seidler, K. Walzer, B. Lüssem, K. Leo, *Nature* **2009**, *459*, 234.
[16] R. Seifert, I. Rabelo de Moraes, S. Scholz, M. C. Gather, B. Lüssem, K. Leo, *Org. Electron.* **2013**, *14*, 115.
[17] S. R. Forrest, *Nature* **2004**, *428*, 911.
[18] S.-M. Lee, J. H. Kwon, S. Kwon, K. C. Choi, *IEEE Trans. Electron Devices* **2017**, *64*, 1922.
[19] S. Scholz, D. Kondakov, B. Lüssem, K. Leo, *Chem. Rev.* **2015**, *115*, 8449.
[20] E. K. Lee, M. Y. Lee, C. H. Park, H. R. Lee, J. H. Oh, *Adv. Mater.* **2017**, *29*, 1703638.
[21] E. G. Jeong, J. H. Kwon, K. S. Kang, S. Y. Jeong, K. C. Choi, *J. Inf. Disp.* **2020**, *21*, 19.
[22] N. Sun, C. Jiang, Q. Li, D. Tan, S. Bi, J. Song, *J. Mater. Sci. Mater. Electron.* **2020**, *31*, 20688.
[23] K. A. Sierros, N. J. Morris, K. Ramji, D. R. Cairns, *Thin Solid Films* **2009**, *517*, 2590.
[24] T. Schwab, S. Schubert, S. Hofmann, M. Fröbel, C. Fuchs, M. Thomschke, L. Müller-Meskamp, K. Leo, M. C. Gather, *Adv. Opt. Mater.* **2013**, *1*, 707.
[25] S. Lenk, T. Schwab, S. Schubert, L. Müller-Meskamp, K. Leo, M. C. Gather, S. Reineke, *Appl. Phys. Lett.* **2015**, *107*, 163302.
[26] S. Schubert, J. Meiss, L. Müller-Meskamp, K. Leo, *Adv. Energy Mater.* **2013**, *3*, 438.
[27] Y. Bi, Y. Liu, X. Zhang, D. Yin, W. Wang, J. Feng, H. Sun, *Adv. Opt. Mater.* **2019**, *7*, 1800778.
[28] D.-Y. Kim, Y. C. Han, H. C. Kim, E. G. Jeong, K. C. Choi, *Adv. Funct. Mater.* **2015**, *25*, 7145.
[29] H. Cho, C. Yun, J. W. Park, S. Yoo, *Org. Electron.* **2009**, *10*, 1163.
[30] S. Kim, J.-L. Lee, *J. Photonics Energy* **2012**, *2*, 021215.
[31] Y. H. Kim, J. Lee, S. Hofmann, M. C. Gather, L. Müller-Meskamp, K. Leo, *Adv. Funct. Mater.* **2013**, *23*, 3763.
[32] S.-I. Na, S.-S. Kim, J. Jo, D.-Y. Kim, *Adv. Mater.* **2008**, *20*, 4061.
[33] T.-H. Han, Y. Lee, M.-R. Choi, S.-H. Woo, S.-H. Bae, B. H. Hong, J.-H. Ahn, T.-W. Lee, *Nat. Photonics* **2012**, *6*, 105.
[34] J. Lee, T.-H. Han, M.-H. Park, D. Y. Jung, J. Seo, H.-K. Seo, H. Cho, E. Kim, J. Chung, S.-Y. Choi, T.-S. Kim, T.-W. Lee, S. Yoo, *Nat. Commun.* **2016**, *7*, 11791.
[35] L.-P. Ma, Z. Wu, L. Yin, D. Zhang, S. Dong, Q. Zhang, M.-L. Chen, W. Ma, Z. Zhang, J. Du, D.-M. Sun, K. Liu, X. Duan, D. Ma, H.-M. Cheng, W. Ren, *Proc. Natl. Acad. Sci. USA* **2020**, *117*, 25991.
[36] D. Zhang, K. Ryu, X. Liu, E. Polikarpov, J. Ly, M. E. Tompson, C. Zhou, *Nano Lett.* **2006**, *6*, 1880.
[37] S. Jiang, P.-X. Hou, M.-L. Chen, B.-W. Wang, D.-M. Sun, D.-M. Tang, Q. Jin, Q.-X. Guo, D.-D. Zhang, J.-H. Du, K.-P. Tai, J. Tan, E. I. Kauppinen, C. Liu, H.-M. Cheng, *Sci. Adv.* **2018**, *4*, eaap9264.
[38] Y. Liu, J. Feng, X.-L. Ou, H. Cui, M. Xu, H.-B. Sun, *Org. Electron.* **2016**, *31*, 247.
[39] W. Gaynor, S. Hofmann, M. G. Christoforo, C. Sachse, S. Mehra, A. Salleo, M. D. McGehee, M. C. Gather, B. Lüssem, L. Müller-Meskamp, P. Peumans, K. Leo, *Adv. Mater.* **2013**, *25*, 4006.
[40] K.-H. Ok, J. Kim, S.-R. Park, Y. Kim, C.-J. Lee, S.-J. Hong, M.-G. Kwak, N. Kim, C. J. Han, J.-W. Kim, *Sci. Rep.* **2015**, *5*, 9464.
[41] A. Takemoto, T. Araki, T. Uemura, Y. Noda, S. Yoshimoto, S. Izumi, S. Tsuruta, T. Sekitani, *Adv. Intell. Syst.* **2020**, *2*, 2000093.
[42] H. B. Lee, W.-Y. Jin, M. M. Ovhal, N. Kumar, J.-W. Kang, *J. Mater. Chem. C* **2019**, *7*, 1087.
[43] J. H. Park, D. Y. Lee, Y.-H. Kim, J. K. Kim, J. H. Lee, J. H. Park, T.-W. Lee, J. H. Cho, *ACS Appl. Mater. Interfaces* **2014**, *6*, 12380.
[44] R.-P. Xu, Y.-Q. Li, J.-X. Tang, *J. Mater. Chem. C* **2016**, *4*, 9116.
[45] S. Sharma, S. Shriwastava, S. Kumar, K. Bhatt, C. C. Tripathi, *Opto-Electron. Rev.* **2018**, *26*, 223.
[46] D. Li, W.-Y. Lai, Y.-Z. Zhang, W. Huang, *Adv. Mater.* **2018**, *30*, 1704738.
[47] M. Morales-Masis, S. De Wolf, R. Woods-Robinson, J. W. Ager, C. Ballif, *Adv. Electron. Mater.* **2017**, *3*, 1600529.
[48] M. S. White, M. Kaltenbrunner, E. D. Głowacki, K. Gutnichenko, G. Kettlgruber, I. Graz, S. Aazou, C. Ulbricht, D. a. M. Egbe, M. C. Miron, Z. Major, M. C. Scharber, T. Sekitani, T. Someya, S. Bauer, N. S. Sariciftci, *Nat. Photonics* **2013**, *7*, 811.
[49] D. Kim, T. Yokota, T. Suzuki, S. Lee, T. Woo, W. Yukita, M. Koizumi, Y. Tachibana, H. Yawo, H. Onodera, M. Sekino, T. Someya, *Proc. Natl. Acad. Sci. USA* **2020**, *2*, 202007395.
[50] E. Kim, J. Kwon, C. Kim, T.-S. Kim, K. C. Choi, S. Yoo, *Org. Electron.* **2020**, *82*, 105704.
[51] Y. Kim, C. Choi, E.-C. Chen, A. G. S. Daniel, A. Masurkar, T. H. Schwartz, H. Ma, I. Kymissis, in *2015 IEEE Int. Electron Devices Meeting*, IEEE, Piscataway, NJ **2015**, pp. 29.6.1–26.6.4.
[52] T. Yokota, P. Zalar, M. Kaltenbrunner, H. Jinno, N. Matsuhisa, H. Kitanosako, Y. Tachibana, W. Yukita, M. Koizumi, T. Someya, *Sci. Adv.* **2016**, *2*, e1501856.
[53] S. Jeong, H. Yoon, B. Lee, S. Lee, Y. Hong, *Adv. Mater. Technol.* **2020**, *5*, 2000231.

[54] D. Yin, N. Jiang, Z. Chen, Y. Liu, Y. Bi, X. Zhang, J. Feng, H. Sun, *Adv. Opt. Mater.* **2020**, *8*, 1901525.
[55] J. Liu, J. Wang, Z. Zhang, F. Molina-Lopez, G.-J. N. Wang, B. C. Schroeder, X. Yan, Y. Zeng, O. Zhao, H. Tran, T. Lei, Y. Lu, Y.-X. Wang, J. B. H. Tok, R. Dauskardt, J. W. Chung, Y. Yun, Z. Bao, *Nat. Commun.* **2020**, *11*, 3362.
[56] J. Liang, L. Li, X. Niu, Z. Yu, Q. Pei, *Nat. Photonics* **2013**, *7*, 817.
[57] D. Yin, J. Feng, R. Ma, Y.-F. Liu, Y.-L. Zhang, X.-L. Zhang, Y.-G. Bi, Q.-D. Chen, H.-B. Sun, *Nat. Commun.* **2016**, *7*, 11573.
[58] M. S. Lim, M. Nam, S. Choi, Y. Jeon, Y. H. Son, S.-M. Lee, K. C. Choi, *Nano Lett.* **2020**, *20*, 1526.
[59] P. E. Burrows, G. L. Graff, M. E. Gross, P. M. Martin, M. K. Shi, M. Hall, E. Mast, C. Bonham, W. Bennett, M. B. Sullivan, *Displays* **2001**, *22*, 65.
[60] J.-S. Park, H. Chae, H. K. Chung, S. I. Lee, *Semicond. Sci. Technol.* **2011**, *26*, 034001.
[61] E. G. Jeong, Y. Jeon, S. H. Cho, K. C. Choi, *Energy Environ. Sci.* **2019**, *12*, 1878.
[62] J. Meyer, P. Görrn, F. Bertram, S. Hamwi, T. Winkler, H. H. Johannes, T. Weimann, P. Hinze, T. Riedl, W. Kowalsky, *Adv. Mater.* **2009**, *21*, 1845.
[63] M.-H. Tseng, H.-H. Yu, K.-Y. Chou, J.-H. Jou, K.-L. Lin, C.-C. Wang, F.-Y. Tsai, *Nanotechnology* **2016**, *27*, 295706.
[64] J. H. Kwon, Y. Jeon, S. Choi, J. W. Park, H. Kim, K. C. Choi, *ACS Appl. Mater. Interfaces* **2017**, *9*, 43983.
[65] E. G. Jeong, S. Kwon, J. H. Han, H.-G. Im, B.-S. Bae, K. C. Choi, *Nanoscale* **2017**, *9*, 6370.
[66] A. Rückerl, R. Zeisel, M. Mandl, I. Costina, T. Schroeder, M. H. Zoellner, *J. Appl. Phys.* **2017**, *121*, 025306.
[67] F. Nehm, H. Klumbies, C. Richter, A. Singh, U. Schroeder, T. Mikolajick, T. Mönch, C. Hoßbach, M. Albert, J. W. Bartha, K. Leo, L. Müller-Meskamp, *ACS Appl. Mater. Interfaces* **2015**, *7*, 22121.
[68] Y. C. Han, C. Jang, K. J. Kim, K. C. Choi, K. Jung, B.-S. Bae, *Org. Electron.* **2011**, *12*, 609.
[69] J. Wu, F. Fei, C. Wei, X. Chen, S. Nie, D. Zhang, W. Su, Z. Cui, *RSC Adv.* **2018**, *8*, 5721.
[70] E. G. Jeong, Y. C. Han, H.-G. Im, B.-S. Bae, K. C. Choi, *Org. Electron.* **2016**, *33*, 150.
[71] Y. C. Han, E. G. Jeong, H. Kim, S. Kwon, H. G. Im, B. S. Bae, K. C. Choi, *RSC Adv.* **2016**, *6*, 40835.
[72] Y. J. Song, J. Kim, H. Cho, Y. H. Son, M. H. Lee, J. Lee, K. C. Choi, S. Lee, *ACS Nano* **2020**, *14*, 1133.
[73] Y. Jeon, H.-R. Choi, J. H. Kwon, S. Choi, K. M. Nam, K.-C. Park, K. C. Choi, *Light: Sci. Appl.* **2019**, *8*, 114.
[74] C. Keum, C. Murawski, E. Archer, S. Kwon, A. Mischok, M. C. Gather, *Nat. Commun.* **2020**, *11*, 6250.
[75] X. Xie, L. Rieth, R. Caldwell, M. Diwekar, P. Tathireddy, R. Sharma, F. Solzbacher, *IEEE Trans. Biomed. Eng.* **2013**, *60*, 2943.
[76] Y. Khan, D. Han, A. Pierre, J. Ting, X. Wang, C. M. Lochner, G. Bovo, N. Yaacobi-Gross, C. Newsome, R. Wilson, A. C. Arias, *Proc. Natl. Acad. Sci. USA* **2018**, *115*, E11015.
[77] H. Lee, E. Kim, Y. Lee, H. Kim, J. Lee, M. Kim, H.-J. Yoo, S. Yoo, *Sci. Adv.* **2018**, *4*, eaas9530.
[78] I. Titov, M. Kopke, N. C. Schneidewind, J. Buhl, Y. Murat, M. Gerken, *IEEE Sens. J.* **2020**, *20*, 7540.
[79] C. Murawski, S. R. Pulver, M. C. Gather, *Nat. Commun.* **2020**, *11*, 6248.
[80] D. Han, Y. Khan, J. Ting, S. M. King, N. Yaacobi-Gross, M. J. Humphries, C. J. Newsome, A. C. Arias, *Adv. Mater.* **2017**, *29*, 1606206.
[81] H. Yun, S. Kim, H. Kim, J. Lee, K. McAllister, J. Kim, S. Pyo, J. Sung Kim, E. E. B. Campbell, W. Hyoung Lee, S. Wook Lee, *Sci. Rep.* **2015**, *5*, 10220.
[82] D. Han, Y. Khan, K. Gopalan, A. Pierre, A. C. Arias, *Adv. Funct. Mater.* **2018**, *28*, 1802986.
[83] K. Hayashi, H. Nakanotani, M. Inoue, K. Yoshida, O. Mikhnenko, T.-Q. Nguyen, C. Adachi, *Appl. Phys. Lett.* **2015**, *106*, 093301.
[84] A. A. Zakhidov, J.-K. Lee, H. H. Fong, J. A. DeFranco, M. Chatzichristidi, P. G. Taylor, C. K. Ober, G. G. Malliaras, *Adv. Mater.* **2008**, *20*, 3481.
[85] P. G. Taylor, J.-K. Lee, A. A. Zakhidov, M. Chatzichristidi, H. H. Fong, J. A. DeFranco, G. G. Malliaras, C. K. Ober, *Adv. Mater.* **2009**, *21*, 2314.
[86] H. Kleemann, A. A. Zakhidov, M. Anderson, T. Menke, K. Leo, B. Lüssem, *Org. Electron.* **2012**, *13*, 506.
[87] S. Krotkus, F. Ventsch, D. Kasemann, A. a. Zakhidov, S. Hofmann, K. Leo, M. C. Gather, *Adv. Opt. Mater.* **2014**, *2*, 1043.
[88] S. Krotkus, D. Kasemann, S. Lenk, K. Leo, S. Reineke, *Light: Sci. Appl.* **2016**, *5*, e16121.
[89] Y. Choi, H. Shin, J. Son, C. Park, K.-W. Park, J.-K. Lee, B. Jung, *Micromachines* **2020**, *11*, 650.
[90] P. E. Malinowski, A. Nakamura, D. Janssen, Y. Kamochi, I. Koyama, Y. Iwai, A. Stefaniuk, E. Wilenska, C. Salas Redondo, D. Cheyns, S. Steudel, P. Heremans, *Org. Electron.* **2014**, *15*, 2355.
[91] C.-Y. Chang, F.-Y. Tsai, S.-J. Jhuo, M.-J. Chen, *Org. Electron.* **2008**, *9*, 667.
[92] S. Choi, C. Kang, C. Byun, H. Cho, B. Kwon, J. Han, J. Yang, J. Shin, C. Hwang, N. S. Cho, K. M. Lee, H.-O. Kim, E. Kim, S. Yoo, H. Lee, *Nat. Commun.* **2020**, *11*, 2732.
[93] F. Ventsch, M. C. Gather, K. Meerholz, *Org. Electron.* **2010**, *11*, 57.
[94] M. C. Gather, A. Köhnen, A. Falcou, H. Becker, K. Meerholz, *Adv. Funct. Mater.* **2007**, *17*, 191.
[95] M. C. Gather, N. M. Kronenberg, K. Meerholz, *Adv. Mater.* **2010**, *22*, 4634.
[96] E. Bodenstein, M. Schober, M. Hoffmann, C. Metzner, U. Vogel, *J. Soc. Inf. Disp.* **2018**, *26*, 555.
[97] W.-J. Joo, J. Kyoung, M. Esfandyarpour, S.-H. Lee, H. Koo, S. Song, Y.-N. Kwon, S. H. Song, J. C. Bae, A. Jo, M. Kwon, S. H. Han, S.-H. Kim, S. Hwang, M. L. Brongersma, *Science* **2020**, *370*, 459.
[98] M. J. J. Coenen, T. M. W. L. Slaats, T. M. Eggenhuisen, P. Groen, *Thin Solid Films* **2015**, *583*, 194.
[99] M. Singh, H. M. Haverinen, P. Dhagat, G. E. Jabbour, *Adv. Mater.* **2010**, *22*, 673.
[100] L. Merklein, D. Daume, F. Braig, S. Schlisske, T. Rödlmeier, M. Mink, D. Kourkoulos, B. Ulber, M. Di Biase, K. Meerholz, G. Hernandez-Sosa, U. Lemmer, H. Sauer, E. Dörsam, P. Scharfer, W. Schabel, *Colloids Interfaces* **2019**, *3*, 32.
[101] A. C, B. Luszczynska, M. Z. Szymanski, J. Ulanski, K. Albrecht, K. Yamamoto, *Org. Electron.* **2019**, *74*, 218.
[102] G. Grau, J. Cen, H. Kang, R. Kitsomboonloha, W. J. Scheideler, V. Subramanian, *Flexible Printed Electron.* **2016**, *1*, 023002.
[103] J. G. Tait, E. Witkowska, M. Hirade, T.-H. Ke, P. E. Malinowski, S. Steudel, C. Adachi, P. Heremans, *Org. Electron.* **2015**, *22*, 40.
[104] N. Strobel, M. Seiberlich, R. Eckstein, U. Lemmer, G. Hernandez-Sosa, *Flexible Printed Electron.* **2019**, *4*, 043001.
[105] Y. Sun, M. Shtein, S. R. Forrest, *Appl. Phys. Lett.* **2005**, *86*, 113504.
[106] G. J. McGraw, D. L. Peters, S. R. Forrest, *Appl. Phys. Lett.* **2011**, *98*, 013302.
[107] G. J. McGraw, S. R. Forrest, *Adv. Mater.* **2013**, *25*, 1583.
[108] J. Li, L. Xu, C. W. Tang, A. A. Shestopalov, *ACS Appl. Mater. Interfaces* **2016**, *8*, 16809.
[109] Y. Tang, Y. Gao, G. Xie, C. Yang, *Nanoscale Horiz.* **2020**, *5*, 144.
[110] J. Choi, K.-H. Kim, S.-J. Choi, H. H. Lee, *Nanotechnology* **2006**, *17*, 2246.
[111] K.-H. Kim, S.-Y. Huh, S.-M. Seo, H. H. Lee, *Org. Electron.* **2008**, *9*, 1118.
[112] A. Carlson, A. M. Bowen, Y. Huang, R. G. Nuzzo, J. A. Rogers, *Adv. Mater.* **2012**, *24*, 5284.
[113] Y. Wada, H. Nakagawa, S. Matsumoto, Y. Wakisaka, H. Kaji, *Nat. Photonics* **2020**, *14*, 643.

[114] M. Y. Wong, E. Zysman-Colman, *Adv. Mater.* **2017**, *29*, 1605444.
[115] H. Kaji, H. Suzuki, T. Fukushima, K. Shizu, K. Suzuki, S. Kubo, T. Komino, H. Oiwa, F. Suzuki, A. Wakamiya, Y. Murata, C. Adachi, *Nat. Commun.* **2015**, *6*, 8476.
[116] X. Wang, R. Wang, D. Zhou, J. Yu, *Synth. Met.* **2016**, *214*, 50.
[117] S. Reineke, M. Thomschke, B. Lüssem, K. Leo, *Rev. Mod. Phys.* **2013**, *85*, 1245.
[118] T.-L. Wu, M.-J. Huang, C.-C. Lin, P.-Y. Huang, T.-Y. Chou, R.-W. Chen-Cheng, H.-W. Lin, R.-S. Liu, C.-H. Cheng, *Nat. Photonics* **2018**, *12*, 235.
[119] X.-K. Liu, C.-J. Zheng, J. Xiao, J. Ye, C.-L. Liu, S.-D. Wang, W.-M. Zhao, X.-H. Zhang, *Phys. Chem. Chem. Phys.* **2012**, *14*, 14255.
[120] K.-H. Kim, S. Lee, C.-K. Moon, S.-Y. Kim, Y.-S. Park, J.-H. Lee, J. W. Lee, J. Huh, Y. You, J.-J. Kim, *Nat. Commun.* **2014**, *5*, 4769.
[121] Z. B. Wang, M. G. Helander, J. Qiu, D. P. Puzzo, M. T. Greiner, Z. M. Hudson, S. Wang, Z. W. Liu, Z. H. Lu, *Nat. Photonics* **2011**, *5*, 753.
[122] Y. Wang, W. Wang, Z. Huang, H. Wang, J. Zhao, J. Yu, D. Ma, *J. Mater. Chem. C* **2018**, *6*, 7042.
[123] M. A. Baldo, C. Adachi, S. R. Forrest, *Phys. Rev. B* **2000**, *62*, 10967.
[124] S. Reineke, K. Walzer, K. Leo, *Phys. Rev. B* **2007**, *75*, 125328.
[125] Y. Zhang, S. Forrest, *Chem. Phys. Lett.* **2013**, *590*, 106.
[126] K. Masui, H. Nakanotani, C. Adachi, *Org. Electron.* **2013**, *14*, 2721.
[127] C. Murawski, K. Leo, M. C. Gather, *Adv. Mater.* **2013**, *25*, 6801.
[128] N. C. Giebink, B. W. D'Andrade, M. S. Weaver, P. B. Mackenzie, J. J. Brown, M. E. Thompson, S. R. Forrest, *J. Appl. Phys.* **2008**, *103*, 044509.
[129] A. S. D. Sandanayaka, T. Matsushima, C. Adachi, *J. Phys. Chem. C* **2015**, *119*, 23845.
[130] J. Lee, C. Jeong, T. Batagoda, C. Coburn, M. E. Thompson, S. R. Forrest, *Nat. Commun.* **2017**, *8*, 15566.
[131] Q. Wang, I. W. H. Oswald, X. Yang, G. Zhou, H. Jia, Q. Qiao, Y. Chen, J. Hoshikawa-Halbert, B. E. Gnade, *Adv. Mater.* **2014**, *26*, 8107.
[132] W. L. Tsai, M. H. Huang, W. K. Lee, Y. J. Hsu, K. C. Pan, Y. H. Huang, H. C. Ting, M. Sarma, Y. Y. Ho, H. C. Hu, C. C. Chen, M. T. Lee, K. T. Wong, C. C. Wu, *Chem. Commun.* **2015**, *51*, 13662.
[133] S. Zou, F. Xie, M. Xie, Y. Li, T. Cheng, X. Zhang, C. Lee, J. Tang, *Adv. Sci.* **2020**, *7*, 1902508.
[134] B. Lüssem, M. Riede, K. Leo, *Phys. Status Solidi A* **2012**, *210*, 9.
[135] M. Pfeiffer, K. Leo, X. Zhou, J. S. Huang, M. Hofmann, A. Werner, J. Blochwitz-Nimoth, *Org. Electron.* **2003**, *4*, 89.
[136] J. Kido, T. Matsumoto, *Appl. Phys. Lett.* **1998**, *73*, 2866.
[137] G. Parthasarathy, C. Shen, A. Kahn, S. R. Forrest, *J. Appl. Phys.* **2001**, *89*, 4986.
[138] Y. Deng, C. Murawski, C. Keum, K. Yoshida, I. D. W. Samuel, M. C. Gather, *Adv. Opt. Mater.* **2020**, *8*, 1901721.
[139] T. Shan, Z. Gao, X. Tang, X. He, Y. Gao, J. Li, X. Sun, Y. Liu, H. Liu, B. Yang, P. Lu, Y. Ma, *Dyes Pigm.* **2017**, *142*, 189.
[140] T. Matsushima, C. Adachi, *Appl. Phys. Lett.* **2008**, *92*, 063306.
[141] L. S. Liao, K. P. Klubek, C. W. Tang, *Appl. Phys. Lett.* **2004**, *84*, 167.
[142] G. He, C. Rothe, S. Murano, A. Werner, O. Zeika, J. Birnstock, *J. Soc. Inf. Disp.* **2009**, *17*, 159.
[143] T.-W. Lee, T. Noh, B.-K. Choi, M.-S. Kim, D. W. Shin, J. Kido, *Appl. Phys. Lett.* **2008**, *92*, 043301.
[144] Y. Jeon, I. Noh, Y. C. Seo, J. H. Han, Y. Park, E. H. Cho, K. C. Choi, *ACS Nano* **2020**, *14*, 15688.
[145] K. Yoshida, P. P. Manousiadis, R. Bian, Z. Chen, C. Murawski, M. C. Gather, H. Haas, G. A. Turnbull, I. D. W. Samuel, *Nat. Commun.* **2020**, *11*, 1171.
[146] K. Yoshida, T. Matsushima, Y. Shiihara, H. Kuwae, J. Mizuno, C. Adachi, *J. Appl. Phys.* **2017**, *121*, 195503.
[147] H. Kuwae, A. Nitta, K. Yoshida, T. Kasahara, T. Matsushima, M. Inoue, S. Shoji, J. Mizuno, C. Adachi, *J. Appl. Phys.* **2015**, *118*, 155501.
[148] A. S. D. Sandanayaka, T. Matsushima, F. Bencheikh, S. Terakawa, W. J. Potscavage, C. Qin, T. Fujihara, K. Goushi, J.-C. Ribierre, C. Adachi, *Appl. Phys. Express* **2019**, *12*, 061010.
[149] D. Kasemann, R. Brückner, H. Fröb, K. Leo, *Phys. Rev. B* **2011**, *84*, 115208.
[150] A. Morton, C. Murawski, Y. Deng, C. Keum, G. B. Miles, J. A. Tello, M. C. Gather, *Adv. Biosyst.* **2019**, *3*, 1800290.
[151] B. F. E. Matarèse, P. L. C. Feyen, J. C. de Mello, F. Benfenati, *Front. Bioeng. Biotechnol.* **2019**, *7*, 278.
[152] W. Brütting, J. Frischeisen, T. D. Schmidt, B. J. Scholz, C. Mayr, *Phys. Status Solidi Appl. Mater. Sci.* **2013**, *210*, 44.
[153] M. C. Gather, S. Reineke, *J. Photonics Energy* **2015**, *5*, 057607.
[154] A. Salehi, X. Fu, D. Shin, F. So, *Adv. Funct. Mater.* **2019**, *29*, 1808803.
[155] J. Song, H. Lee, E. G. Jeong, K. C. Choi, S. Yoo, *Adv. Mater.* **2020**, *32*, 1907539.
[156] J. Shinar, R. Shinar, *J. Phys. D. Appl. Phys.* **2008**, *41*, 133001.
[157] D. A. Bernards, R. M. Owens, G. G. Malliaras, *Organic Semiconductors in Sensor Applications*, Springer, Berlin **2008**.
[158] F. Krujatz, O. Hild, K. Fehse, J. M, A. Werner, T. Bley, *Chem. Sci. J.* **2016**, *7*, 134.
[159] F. Lefèvre, P. Juneau, R. Izquierdo, *Sens. Actuators, B* **2015**, *221*, 1314.
[160] M. C. Gather, F. Ventsch, K. Meerholz, *Adv. Mater.* **2008**, *20*, 1966.
[161] Y. Ohmori, M. Hikita, H. Kajii, T. Tsukagawa, K. Yoshino, M. Ozaki, A. Fujii, S. Tomaru, S. Imamura, H. Takenaka, J. Kobayashi, F. Yamamoto, *Thin Solid Films* **2001**, *393*, 267.
[162] Y. Ohmori, H. Kajii, M. Kaneko, K. Yoshino, M. Ozaki, A. Fujii, M. Hikita, H. Takenaka, T. Taneda, *IEEE J. Sel. Top. Quantum Electron.* **2004**, *10*, 70.
[163] R. Liu, R. Ishimatsu, M. Yahiro, C. Adachi, K. Nakano, T. Imato, *Talanta* **2015**, *132*, 96.
[164] V. Venkatraman, A. J. Steckl, *IEEE Sens. J.* **2017**, *17*, 8343.
[165] S. Jahns, A. F. K. Iwers, J. Balke, M. Gerken, *tm – Tech. Mess.* **2017**, *84*, 48.
[166] A. Banerjee, Y. Shuai, R. Dixit, I. Papautsky, D. Klotzkin, *J. Lumin.* **2010**, *130*, 1095.
[167] H. Nakajima, Y. Okuma, K. Morioka, M. Miyake, A. Hemmi, T. Tobita, M. Yahiro, D. Yokoyama, C. Adachi, N. Soh, K. Nakano, S. Xue, H. Zeng, K. Uchiyama, T. Imato, *J. Sep. Sci.* **2011**, *34*, 2906.
[168] R. Liu, R. Ishimatsu, M. Yahiro, C. Adachi, K. Nakano, T. Imato, *Talanta* **2015**, *134*, 37.
[169] Z. Shu, F. Kemper, E. Beckert, R. Eberhardt, A. Tünnermann, *RSC Adv.* **2017**, *7*, 26384.
[170] A. Marcello, D. Sblattero, C. Cioarec, P. Maiuri, P. Melpignano, *Biosens. Bioelectron.* **2013**, *46*, 44.
[171] F. Lefèvre, A. Chalifour, L. Yu, V. Chodavarapu, P. Juneau, R. Izquierdo, *Lab Chip* **2012**, *12*, 787.
[172] A. Pais, A. Banerjee, D. Klotzkin, I. Papautsky, *Lab Chip* **2008**, *8*, 794.
[173] B. A. Katchman, J. T. Smith, U. Obahiagbon, S. Kesiraju, Y. Lee, B. O'Brien, K. Kaftanoglu, J. B. Christen, K. S. Anderson, *Sci. Rep.* **2016**, *6*, 29057.
[174] B. Yao, G. Luo, L. Wang, Y. Gao, G. Lei, K. Ren, L. Chen, Y. Wang, Y. Hu, Y. Qiu, *Lab Chip* **2005**, *5*, 1041.
[175] S. Vengasandra, Y. Cai, D. Grewell, J. Shinar, R. Shinar, *Lab Chip* **2010**, *10*, 1051.
[176] A. Acharya, M. Packirisamy, R. Izquierdo, *Micromachines* **2015**, *6*, 1406.
[177] A. Banerjee, A. Pais, I. Papautsky, D. Klotzkin, *IEEE Sens. J.* **2008**, *8*, 621.
[178] V. Venkatraman, A. J. Steckl, *Biosens. Bioelectron.* **2015**, *74*, 150.
[179] C. Murawski, A. Mischok, J. Booth, J. D. Kumar, E. Archer, L. Tropf, C. Keum, Y. Deng, K. Yoshida, I. D. W. Samuel, M. Schubert, S. R. Pulver, M. C. Gather, *Adv. Mater.* **2019**, *31*, 1903599.
[180] T. Hatakeyama, K. Shiren, K. Nakajima, S. Nomura, S. Nakatsuka, K. Kinoshita, J. Ni, Y. Ono, T. Ikuta, *Adv. Mater.* **2016**, *28*, 2777.

[181] Y. Kondo, K. Yoshiura, S. Kitera, H. Nishi, S. Oda, H. Gotoh, Y. Sasada, M. Yanai, T. Hatakeyama, *Nat. Photonics* **2019**, *13*, 678.
[182] T. Fleetham, G. Li, L. Wen, J. Li, *Adv. Mater.* **2014**, *26*, 7116.
[183] T. Fleetham, J. H. Golden, M. Idris, H. Hau, D. S. Muthiah Ravinson, P. I. Djurovich, M. E. Thompson, *Inorg. Chem.* **2019**, *58*, 12348.
[184] G. Li, T. Fleetham, E. Turner, X.-C. Hang, J. Li, *Adv. Opt. Mater.* **2015**, *3*, 390.
[185] M. Jahnel, B. Beyer, M. Thomschke, K. Fehse, F. Krujatz, K. Leo, *Electronics* **2015**, *4*, 982.
[186] C.-M. Keum, N. M. Kronenberg, C. Murawski, K. Yoshida, Y. Deng, C. Berz, W. Li, M. Wei, I. D. W. Samuel, M. C. Gather, *Adv. Opt. Mater.* **2018**, *6*, 1800496.
[187] Y. Deng, C. Keum, S. Hillebrandt, C. Murawski, M. C. Gather, *Adv. Opt. Mater.* **2020**, 2001642, https://doi.org/10.1002/adom.202001642.
[188] B. Siegmund, A. Mischok, J. Benduhn, O. Zeika, S. Ullbrich, F. Nehm, M. Böhm, D. Spoltore, H. Fröb, C. Körner, K. Leo, K. Vandewal, *Nat. Commun.* **2017**, *8*, 15421.
[189] Y. Fang, Q. Dong, Y. Shao, Y. Yuan, J. Huang, *Nat. Photonics* **2015**, *9*, 679.
[190] H.-S. Rao, W.-G. Li, B.-X. Chen, D.-B. Kuang, C.-Y. Su, *Adv. Mater.* **2017**, *29*, 1602639.
[191] M. I. Saidaminov, M. A. Haque, M. Savoie, A. L. Abdelhady, N. Cho, I. Dursun, U. Buttner, E. Alarousu, T. Wu, O. M. Bakr, *Adv. Mater.* **2016**, *28*, 8144.
[192] J. Li, J. Wang, J. Ma, H. Shen, L. Li, X. Duan, D. Li, *Nat. Commun.* **2019**, *10*, 806.
[193] D. Li, G. Dong, W. Li, L. Wang, *Sci. Rep.* **2015**, *5*, 7902.
[194] H. Guo, J. Zhao, Q. Dong, L. Wang, X. Ren, S. Liu, C. Zhang, G. Dong, *Nano Energy* **2019**, *56*, 391.
[195] E. López-Fraguas, B. Arredondo, C. Vega-Colado, G. del Pozo, M. Najafi, D. Martín-Martín, Y. Galagan, J. M. Sánchez-Pena, R. Vergaz, B. Romero, *Org. Electron.* **2019**, *73*, 292.
[196] A. T. Exner, I. Pavlichenko, D. Baierl, M. Schmidt, G. Derondeau, B. V. Lotsch, P. Lugli, G. Scarpa, *Laser Photonics Rev.* **2014**, *8*, 726.
[197] F. Krujatz, K. Fehse, M. Jahnel, C. Gommel, C. Schurig, F. Lindner, T. Bley, J. Weber, J. Steingroewer, *Algal Res.* **2016**, *18*, 225.
[198] Z. Shu, O. Pabst, E. Beckert, R. Eberhardt, A. Tünnermann, *Proc. SPIE* **2016**, *9745*, p. 97450W.
[199] M. Koetse, P. Rensing, G. van Heck, R. Sharpe, B. Allard, F. Wieringa, P. Kruijt, N. Meulendijks, H. Jansen, H. Schoo, *Proc. SPIE* **2008**, *7054*, 70541I.
[200] M. M. Koetse, P. A. Rensing, G. T. van Heck, N. N. M. M. Meulendijks, P. G. M. Kruijt, E. H. Enting, F. P. Wieringa, H. F. M. Schoo, in *2008 IEEE Sensors Applications Symp.*, IEEE, Atlanta, GA, USA **2008**, pp. 1–3, 10.1109/SAS13374.2008.4472931.
[201] F. Elsamnah, A. Bilgaiyan, M. Affiq, C.-H. Shim, H. Ishidai, R. Hattori, *Biosensors* **2019**, *9*, 48.
[202] F. Elsamnah, A. Bilgaiyan, M. Affiq, C.-H. Shim, H. Ishidai, R. Hattori, *Biosensors* **2019**, *9*, 87.
[203] A. Bilgaiyan, F. Elsamnah, H. Ishidai, C.-H. Shim, M. A. Bin Misran, C. Adachi, R. Hattori, *ACS Appl. Electron. Mater.* **2020**, *2*, 1280.
[204] C. M. Lochner, Y. Khan, A. Pierre, A. C. Arias, *Nat. Commun.* **2014**, *5*, 5745.
[205] Y. Lee, H. Lee, J. Jang, J. Lee, M. Kim, J. Lee, H. Kim, S. Yoo, H. J. Yoo, *IEEE J. Emerging Sel. Top. Circuits Syst.* **2017**, *7*, 50.
[206] D. Han, Y. Khan, J. Ting, J. Zhu, C. Combe, A. Wadsworth, I. McCulloch, A. C. Arias, *Adv. Mater. Technol.* **2020**, *5*, 1901122.
[207] A. K. Bansal, S. Hou, O. Kulyk, E. M. Bowman, I. D. W. Samuel, *Adv. Mater.* **2015**, *27*, 7638.
[208] S. D. Yambem, T. L. Brooks-Richards, D. P. Forrestal, M. Kielar, P. Sah, A. K. Pandey, M. A. Woodruff, *Sci. Rep.* **2019**, *9*, 9875.
[209] D. E. J. G. J. Dolmans, D. Fukumura, R. K. Jain, *Nat. Rev. Cancer* **2003**, *3*, 380.
[210] B. Liu, S. Monro, Z. Li, M. A. Jabed, D. Ramirez, C. G. Cameron, K. Colón, J. Roque, S. Kilina, J. Tian, S. A. McFarland, W. Sun, *ACS Appl. Bio Mater.* **2019**, *2*, 2964.
[211] J. Zhang, W. Chen, R. Chen, X. Liu, Y. Xiong, S. V. Kershaw, A. L. Rogach, C. Adachi, X. Zhang, C. Lee, *Chem. Commun.* **2016**, *52*, 11744.
[212] J. Zhang, F. Fang, B. Liu, J.-H. Tan, W.-C. Chen, Z. Zhu, Y. Yuan, Y. Wan, X. Cui, S. Li, Q.-X. Tong, J. Zhao, X.-M. Meng, C.-S. Lee, *ACS Appl. Mater. Interfaces* **2019**, *11*, 41051.
[213] Z. Liu, F. Song, W. Shi, G. Gurzadyan, H. Yin, B. Song, R. Liang, X. Peng, *ACS Appl. Mater. Interfaces* **2019**, *11*, 15426.
[214] H. Abrahamse, M. R. Hamblin, *Biochem. J.* **2016**, *473*, 347.
[215] B. Wang, L. Shi, Y. F. Zhang, Q. Zhou, J. Zheng, R. M. Szeimies, X. L. Wang, *Br. J. Dermatol.* **2017**, *177*, 656.
[216] S. K. Attili, A. Lesar, A. McNeill, M. Camacho-Lopez, H. Moseley, S. Ibbotson, I. D. W. Samuel, J. Ferguson, *Br. J. Dermatol.* **2009**, *161*, 170.
[217] H.-W. Guo, L.-T. Lin, P.-H. Chen, M.-H. Ho, W.-T. Huang, Y.-J. Lee, S.-H. Chiou, Y.-S. Hsieh, C.-Y. Dong, H.-W. Wang, *Photodiagn. Photodyn. Ther.* **2015**, *12*, 504.
[218] C. Lian, M. Piksa, K. Yoshida, S. Persheyev, K. J. Pawlik, K. Matczyszyn, I. D. W. Samuel, *npj Flexible Electron.* **2019**, *3*, 18.
[219] C. Mignon, N. V. Botchkareva, N. E. Uzunbajakava, D. J. Tobin, *Exp. Dermatol.* **2016**, *25*, 745.
[220] L. F. de Freitas, M. R. Hamblin, *IEEE J. Sel. Top. Quantum Electron.* **2016**, *22*, 348.
[221] X. Wu, S. Alberico, E. Saidu, S. Rahman Khan, S. Zheng, R. Romero, H. Sik Chae, S. Li, A. Mochizuki, J. Anders, *Wound Repair Regener.* **2015**, *23*, 104.
[222] S. Mo, P. S. Chung, J. C. Ahn, *Curr. Opt. Photonics* **2019**, *3*, 485.
[223] Y. Jeon, H.-R. Choi, M. Lim, S. Choi, H. Kim, J. H. Kwon, K.-C. Park, K. C. Choi, *Adv. Mater. Technol.* **2018**, *3*, 1700391.
[224] Y. Jeon, H. Choi, K. Park, K. C. Choi, *J. Soc. Inf. Disp.* **2020**, *28*, 324.
[225] J. N. Sahni, G. Czanner, T. Gutu, S. A. Taylor, K. M. Bennett, S. M. Wuerger, I. Grierson, C. Murray-Dunning, M. N. Holland, S. P. Harding, *Eye* **2017**, *31*, 97.
[226] I. Jun, S. J. Han, H.-S. Shin, J. Kim, E. K. Kim, T. Kim, S. C. Yoon, K. Y. Seo, *Sci. Rep.* **2020**, *10*, 11582.
[227] E. S. Boyden, F. Zhang, E. Bamberg, G. Nagel, K. Deisseroth, *Nat. Neurosci.* **2005**, *8*, 1263.
[228] S. Jarrin, D. P. Finn, *Neurosci. Biobehav. Rev.* **2019**, *105*, 200.
[229] J. G. Bernstein, E. S. Boyden, *Trends Cognit. Sci.* **2011**, *15*, 592.
[230] H. F. Iaccarino, A. C. Singer, A. J. Martorell, A. Rudenko, F. Gao, T. Z. Gillingham, H. Mathys, J. Seo, O. Kritskiy, F. Abdurrob, C. Adaikkan, R. G. Canter, R. Rueda, E. N. Brown, E. S. Boyden, L.-H. Tsai, *Nature* **2016**, *540*, 230.
[231] K. M. Tye, K. Deisseroth, *Nat. Rev. Neurosci.* **2012**, *13*, 251.
[232] J. A. Steinbeck, S. J. Choi, A. Mrejeru, Y. Ganat, K. Deisseroth, D. Sulzer, E. V. Mosharov, L. Studer, *Nat. Biotechnol.* **2015**, *33*, 204.
[233] R. A. B. Burton, A. Klimas, C. M. Ambrosi, J. Tomek, A. Corbett, E. Entcheva, G. Bub, *Nat. Photonics* **2015**, *9*, 813.
[234] U. Nussinovitch, L. Gepstein, *Nat. Biotechnol.* **2015**, *33*, 750.
[235] A. D. Mickle, S. M. Won, K. N. Noh, J. Yoon, K. W. Meacham, Y. Xue, L. A. McIlvried, B. A. Copits, V. K. Samineni, K. E. Crawford, D. H. Kim, P. Srivastava, B. H. Kim, S. Min, Y. Shiuan, Y. Yun, M. A. Payne, J. Zhang, H. Jang, Y. Li, H. H. Lai, Y. Huang, S.-I. Park, R. W. Gereau, J. A. Rogers, *Nature* **2019**, *565*, 361.
[236] A. Dieter, D. Keppeler, T. Moser, *EMBO Mol. Med.* **2020**, *12*, 11618.
[237] D. Keppeler, M. Schwaerzle, T. Harczos, L. Jablonski, A. Dieter, B. Wolf, S. Ayub, C. Vogl, C. Wrobel, G. Hoch, K. Abdellatif, M. Jeschke, V. Rankovic, O. Paul, P. Ruther, T. Moser, *Sci. Transl. Med.* **2020**, *12*, eabb8086.
[238] V. Busskamp, S. Picaud, J. A. Sahel, B. Roska, *Gene Ther.* **2012**, *19*, 169.
[239] M. P. Simunovic, W. Shen, J. Y. Lin, D. A. Protti, L. Lisowski, M. C. Gillies, *Exp. Eye Res.* **2019**, *178*, 15.

[240] A. M. Packer, B. Roska, M. Häusser, *Nat. Neurosci.* **2013**, *16*, 805.
[241] A. Ghosh, E. P. Donoghue, I. Khayrullin, T. Ali, I. Wacyk, K. Tice, F. Vazan, L. Sziklas, D. Fellowes, R. Draper, *SID Symp. Dig. Tech. Pap.* **2016**, *47*, 837.
[242] F. Fries, M. Fröbel, S. Lenk, S. Reineke, *Org. Electron.* **2017**, *41*, 315.
[243] J. Lee, S. Hofmann, M. Furno, M. Thomschke, Y. H. Kim, B. Lüssem, K. Leo, *Org. Electron.* **2011**, *12*, 1383.
[244] M. Fröbel, T. Schwab, M. Kliem, S. Hofmann, K. Leo, M. C. Gather, *Light: Sci. Appl.* **2015**, *4*, e247.
[245] T. D. Y. Kozai, A. S. Jaquins-Gerstl, A. L. Vazquez, A. C. Michael, X. T. Cui, *ACS Chem. Neurosci.* **2015**, *6*, 48.
[246] N. C. Klapoetke, Y. Murata, S. S. Kim, S. R. Pulver, A. Birdsey-Benson, Y. K. Cho, T. K. Morimoto, A. S. Chuong, E. J. Carpenter, Z. Tian, J. Wang, Y. Xie, Z. Yan, Y. Zhang, B. Y. Chow, B. Surek, M. Melkonian, V. Jayaraman, M. Constantine-Paton, G. K.-S. Wong, E. S. Boyden, *Nat. Methods* **2014**, *11*, 338.
[247] A. Dawydow, R. Gueta, D. Ljaschenko, S. Ullrich, M. Hermann, N. Ehmann, S. Gao, A. Fiala, T. Langenhan, G. Nagel, R. J. Kittel, *Proc. Natl. Acad. Sci. USA* **2014**, *111*, 13972.
[248] A. Steude, M. Jahnel, M. Thomschke, M. Schober, M. C. Gather, *Adv. Mater.* **2015**, *27*, 7657.
[249] A. Steude, E. C. Witts, G. B. Miles, M. C. Gather, *Sci. Adv.* **2016**, *2*, e1600061.
[250] A. Morton, C. Murawski, S. R. Pulver, M. C. Gather, *Sci. Rep.* **2016**, *6*, 31117.
[251] I. Meloni, D. Sachidanandan, A. S. Thum, R. J. Kittel, C. Murawski, *Sci. Rep.* **2020**, *10*, 17614.
[252] A. Sridharan, A. Shah, S. S. Kumar, J. Kyeh, J. Smith, J. Blain-Christen, J. Muthuswamy, *Biomed. Phys. Eng. Express* **2020**, *6*, 025003.
[253] S. Rezaei-Mazinani, A. I. Ivanov, C. M. Proctor, P. Gkoupidenis, C. Bernard, G. G. Malliaras, E. Ismailova, *Adv. Mater. Technol.* **2018**, *3*, 1700333.
[254] S. Rezaei-Mazinani, A. I. Ivanov, M. Biele, A. L. Rutz, V. G. Gregoriou, A. Avgeropoulos, S. F. Tedde, C. L. Chochos, C. Bernard, R. P. O'Connor, G. G. Malliaras, E. Ismailova, *J. Mater. Chem. C* **2019**, *7*, 9049.
[255] M. Kielar, H. Gooch, L. Xu, A. K. Pandey, P. Sah, *ACS Photonics* **2021**, *8*, 228.
[256] P. C. Y. Chow, T. Someya, *Adv. Mater.* **2020**, *32*, 1902045.
[257] H. Ren, J. Chen, Y. Li, J. Tang, *Adv. Sci.* **2020**, *14*, 2002418.
[258] Z. Zhao, C. Xu, L. Niu, X. Zhang, F. Zhang, *Laser Photonics Rev.* **2020**, *14*, 2000262.
[259] Z. Chen, S. N. Obaid, L. Lu, *Opt. Mater. Express* **2019**, *9*, 3843.
[260] T. Someya, Z. Bao, G. G. Malliaras, *Nature* **2016**, *540*, 379.
[261] J. Hopkins, L. Travaglini, A. Lauto, T. Cramer, B. Fraboni, J. Seidel, D. Mawad, *Adv. Mater. Technol.* **2019**, *4*, 1800744.
[262] J. Rivnay, S. Inal, A. Salleo, R. M. Owens, M. Berggren, G. G. Malliaras, *Nat. Rev. Mater.* **2018**, *3*, 17086.
[263] A. Buckley, I. Underwood, C. J. Yates, in A. Buckley, The technology and manufacturing of polymer OLED on complementary metal oxide semiconductor (CMOS) microdisplays. *Organic Light-Emitting Diodes*, Woodhead Publishing, **2013**, pp. 459–511.
[264] I. Wacyk, A. Ghosh, O. Prache, R. Draper, D. A. Fellowes, *in Proc. SPIE* **2012**, *8383*, 83830Q.
[265] T. Maindron, B. Chambion, M. Provost, A. Vandeneynde, P. Peray, M. Zussy, J. Dechamp, C. Rossat, S. Gonnin, *J. Soc. Inf. Disp.* **2019**, *27*, 723.
[266] U. Vogel, P. Wartenberg, B. Richter, S. Brenner, J. Baumgarten, M. Thomschke, K. Fehse, O. Hild, *Proc. SPIE* **2015**, *9626*, 96263I.

Caroline Murawski obtained a Ph.D. in physics from TU Dresden, Germany, in 2015. Her Ph.D. research focused on efficiency roll-off of organic LEDs under guidance of Prof. Karl Leo. As Marie Curie Fellow, she did postdoctoral research at the University of St Andrews, UK, from 2015 to 2018. Since 2018, she is working as independent research group leader at Kurt-Schwabe-Institut Meinsberg, Germany. Her research revolves around novel designs and applications of organic electronics in biophotonics, medicine, and sensing.

Malte C. Gather works at the interface between biophotonics and organic semiconductors, with particular focus on resonant and implantable devices. After a Ph.D. on organic LEDs in 2008, he was a postdoc at University of Iceland and later at Harvard University, USA, where he developed the first laser based on a live cell. He was an assistant professor at TU Dresden, Germany, working with Prof. Karl Leo, from 2011 to 2013 before becoming a full professor at University of St Andrews, UK. He recently won the Alexander von Humboldt Professorship to set up a new research center for nano- and biophotonics at University of Cologne, Germany.